File.

I.O.S.

INTERNAL DOCUMENT

89

MAIN COMPUTATION NETWORK

A part of the electronic model
for tides and storm surges

S. Ishiguro

1973*

[This document should not be cited in a published bibliography, and is supplied for the use of the recipient only].

NATURAL ENVIRONMENT RESEARCH COUNCIL
INSTITUTE OF OCEANOGRAPHIC SCIENCES

INSTITUTE OF OCEANOGRAPHIC SCIENCES

Wormley, Godalming,
Surrey, GU8 5UB.
(042-879-4141)

(Director: Dr. A. S. Laughton)

Bidston Observatory,
Birkenhead,
Merseyside, L43 7RA.
(051-652-2396)
(Assistant Director: Dr. D. E. Cartwright)

Crossway,
Taunton,
Somerset, TA1 2DW.
(0823-86211)
(Assistant Director: M.J. Tucker)

INSTITUTE OF OCEANOGRAPHIC SCIENCES

INTERNAL REPORT 89

MAIN COMPUTATION NETWORK

A part of the electronic model
for tides and storm surges

S. Ishiguro

1973*

* The scritp of this paper was written in 1973, but only two copies were made at that time. Since the recent papers of this project are required to refer to this paper, its copies have been added to this series.

Alterations have only been made on this occasion to Page 2, chapter numbers and page numbers. (1980)

46 pages, 32 diagrams, 6 tables

INSTITUTE OF OCEANOGRAPHIC SCIENCES, WORMLEY

CONTENTS

	Abstract	2
1.	Introduction	2
2.	Outline of the whole model system	3
3.	Some equations relating to the model	5
4.	Examples of the model parameters	9
5.	Fundamantal design	11
6.	Opto-electronic coupling	13
7.	Electronic design	17
8.	Physical design	22
9.	Floating DC-power supply	24
10.	Performance	28
11.	Conclusion	37
	Acknowledgements	37
	Appendices 1 to 6	38-46

ABSTRACT

The electronic model for tides and storm surges has a large number of 'grid cards' each of which represents a quantized hydrodynamic system of the rotating sea with external forces. All the grid cards have an electrically and physically idential construction, but each card can store different time-independent variables of the system, while its time-dependent variables are fed into the grid from another circuit. This technique offers the solution of the dynamic equations without a step-by-step process (which is inherent in a digital technique) and high speed processing (typically 10 milli secons for a 10-day sotrm surge). Described in this paper is the design of such grid cards with floating DC-power supply units.

1. INTRODUCTION

The first two-dimansional non-steady state rotational electronic model for tides and storm surges was introduced by the author in 1956. This was an electronic network (called 'Main Computation Network') which has a quantitative analogy to the hydrodynamic system of tides/surge phenomena. The time-independent variables of the system are stored in the network, and the voltages representing its time-dependent variables are fed into the network simultaneously from a multiple function generator.

This technique offers the solution of the dynamic equations without a step-by-step process (which is inherent in a digital technique) and overcomes problems of computational instability which can arise in a step-by-step method. The technique also facilitates a speedy computation.

In the ealier model, analogue techniques were employed for both the computation network and function generator. In the recent model, more advanced analogue electronic techniques have been applied to the network, and digital techniques to the rest of the circuits including the function generator. Described in this paper is the design of 'grid cards' which are the 'building blocks' of the computation network.

Note The principle of the computation network is an original idea (patented). Although this circuit is an electronic analogue circuit in the sense of being non-digital, this is not related to an analogue computer consisting of operational amplifiers with feed-back elements.

2. OUTLINE OF THE WHOLE MODEL SYSTEM

Fig. 1 shows a simplified schematic diagram of the whole model system.

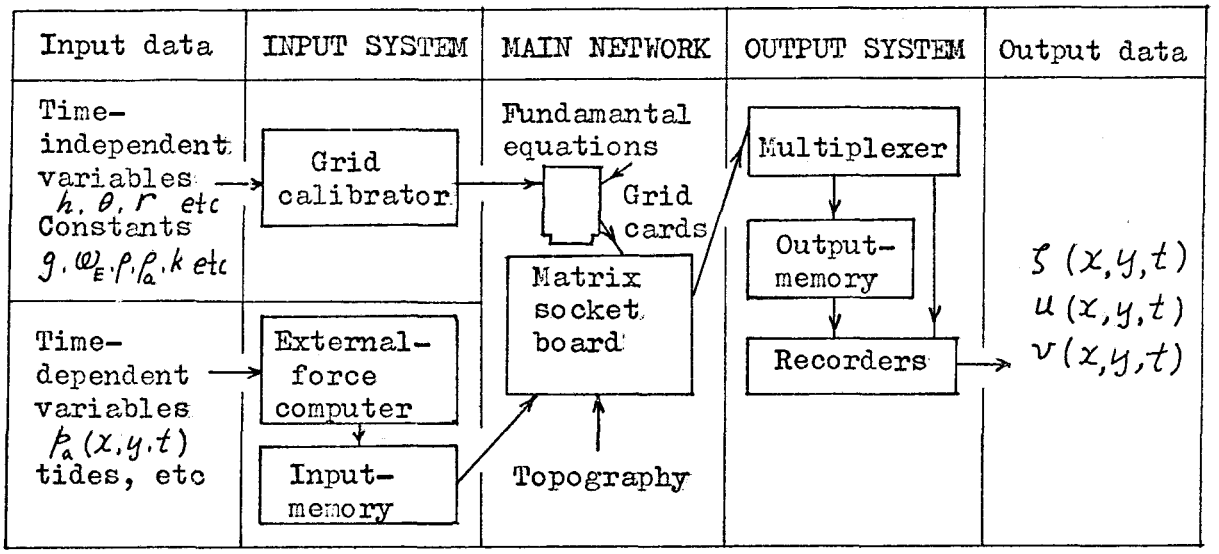

Fig. 1. Simplified schematic diagram of the whole system.

The MAIN NETWORK consists of a number of grid cards and a matrix socket board with a floating dc-power supply. Each grid card represents a unit section of the quantized hydrodynamic system of the rotating sea whose characteristics are defined by the fundamental equations (Chapter 2), e.g. linear or non-linear (the linear version only has been made). Different types of grid can be used in combination, providing their electronic and physical specifications are matched with related parts. The matrix socket board has been provided for combining all the grids so that an arbitrary topography of the sea can be modelled.

The INPUT SYSTEM consists of three major parts: a grid-card calibrator, an external-force computer and an input memory. The grid-card calibrator has been prepared for setting the time-independent input data into each grid card. Generally the data for an atmospheric pressure field are given in the form of $p_a(x,y,t)$, and the wind field has to be computed from them assuming a geostrophic wind. Then, from these two types of data, the resultant of 'pressure disturbance' $\xi_p(x,y,t)$ and 'wind disturbance' $\xi_w(x,y,t)$ within each grid should be computed. The external-force computer has been prepared to carry out this operation, simultaneously when the input data are received. The computed input data are stored by the input memory, and are fed into each grid simultaneously at an appropriate speed through the matrix socket board of the MAIN NETWORK. Other types of input data, such as tides, can be accessed directly by the same memory.

The OUTPUT SYSTEM has been prepared for recording the output data which are available simultaneously from the grids. In order to economize the recorders, a multiplexer has been used. Since the full computation takes only 10 ms typically, this is repeated as many times as required for recording. The output memory can store a small amount of output data temporarily so that the data-feeding speed for the recorders can be adjusted.

The total processing time of the system is determined in practice by the speed of the external input-data feeding apparatus, e.g. a keyboard, punched-tape reader, magnetic-tape reader or direct data-line. A typical speed would be 56 sec for an 8-day surge period by a 500 ch/s tape reader, or 134 ms with the maximum data-feeding speeed of 100K ch/s.

The numerical accuracy (which excludes the accuracy in representation of the real phenomena by the fundamental equations), stability and linearity have been designed to be better than ± 1.6% of the full scale of variables.

The input of the system is digital, and the output of the system is digital and analogue, e.g. a numerical printer, tape punch, and XYT plotter. The analogue output can be monitored by a CRO. The intermediate stages of the system are hybrid of digital and analogue. The whole system consists of about 1.2 million transistors; 97% for digital circuits, and 3% for analogue circuits. 330 grid cards have been made so far, while the cabinet of the MAIN NETWORK has a capacity of 990 grid cards.

3. SOME EQUATIONS RELATING TO THE MODEL

Electronic equations listed here are limited to those directly related with the hydrodynamic system.

Symbols

Hydrodynamic system:

x, y	Cartesian cordinates
$\Delta x, \Delta y$	Finite increments of x and y (not necessarily equal)
t	Time
ζ	Elevation of water surface
h	Depth of undisturbed water
U	Velocity of water current (suffix b for the sea bottom)
u, v	x and y components of U
W_x, W_y	x and y xomponents of volume transport of water
U_a	Velocity of wind on the water surface
u_a, v_a	x and y component of U_a
p	Atmospheric pressure on the water surface
τ_{bx}, τ_{by}	x and y components of stress on the sea bottom
τ_{ax}, τ_{ay}	x and y components of stress on the sea surface
X, Y	x and y components of other external force
ρ	Density of water (assumed uniform) = 1.03 gr cm^{-3}
ρ_a	Density of air = 1.25×10^{-3} gr cm^{-3}
k	Coefficient (relating to friction) = 2.5×10^{-3}
ϕ	Latitude
ω_E	Angular speed of the earth's rotation = 7.292×10^{-5} s^{-1}
g	Acceleration of the earth's gravity = 9.81×10^{2} cm s^{-1}
β	Coefficient (relating to geostrophic wind, dimensionless)
δ	Backing angle of wind direction) (relating to geostrophic-wind estimation)

Electronic system:

t_e	Time in the model
T_e	Period in the model
e	Voltage
i	Current
R	Resistance
L	Inductance
C	Capacitance
Z	Impedance
Ω_e	Coriolis parameter in the model (unit in ohms)

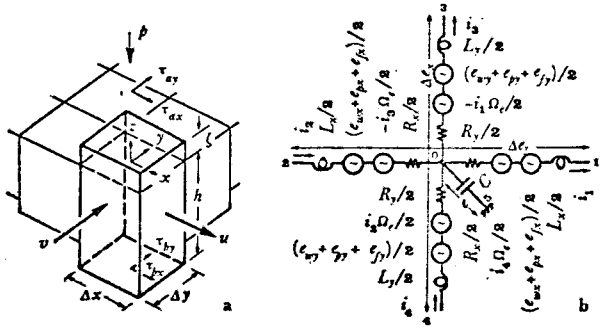

Fig. 2. Discrete representation of rotating two-dimensional hydrodynamic system and its analogue circuit. A signal grid only is shown.

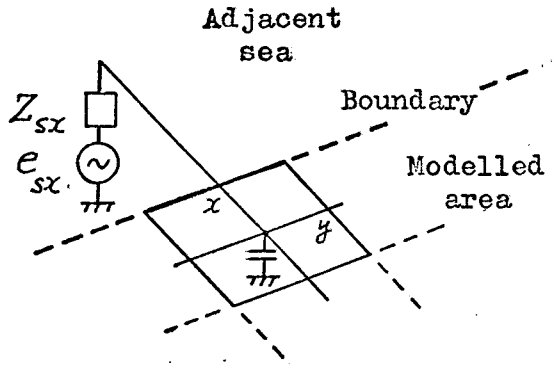

Fig. 3. Termination of a grid representing the boundary between a modelled area and an adjacent sea.

Hydrodynamic equations for tides and storm surges in a rotating sea

$$-\Delta x \frac{\partial \zeta}{\partial x} = \frac{1}{gh} \frac{\Delta x}{\Delta y} \frac{\partial W_x}{\partial t} - \frac{\Omega W_y}{gh} + \frac{\Delta x \tau_{bx}}{\rho g h} - \frac{\Delta x \tau_{ax}}{\rho g h} + \frac{\Delta x}{\rho g} \frac{\partial p}{\partial x} + \frac{\Delta x \cdot X}{g} \quad (1)$$

$$\Delta y \frac{\partial \zeta}{\partial y} = \frac{1}{gh} \frac{\Delta y}{\Delta x} \frac{\partial W_y}{\partial t} + \frac{\Omega W_x}{gh} + \frac{\Delta y \tau_{by}}{\rho g h} - \frac{\Delta y \tau_{ay}}{\rho g h} + \frac{\Delta y}{\rho g} \frac{\partial p}{\partial y} + \frac{\Delta y \cdot Y}{g} \quad (2)$$

$$-\frac{\partial \zeta}{\partial t} = \frac{1}{\Delta y} \frac{\partial W_x}{\partial x} + \frac{1}{\Delta x} \frac{\partial W_y}{\partial y} \quad (3)$$

$$W_x = \int_{-h}^{0} \int_{-\Delta y/2}^{\Delta y/2} u \cdot dz \cdot dy$$
$$W_y = \int_{-h}^{0} \int_{-\Delta x/2}^{\Delta x/2} v \cdot dz \cdot dx \quad (4)$$

$$\Omega = 2 \omega_E \sin \phi \quad (5)$$

$$\tau_{bx} = \rho k u_b |U| \qquad \tau_{by} = \rho k v_b |U| \quad (6)$$

$$\tau_{ax} = \rho_a k u_a |U_a| \qquad \tau_{ay} = \rho_a k v_a |U_a| \quad (7)$$

Electronic equations for a grid card (linear version)

$$-\Delta e_x = L_x \frac{\partial i_x}{\partial t_e} - \Omega_e i_y + R_x i_x + (-e_{wx} + e_{px} + e_{fx}) \quad (8)$$

$$-\Delta e_y = L_y \frac{\partial i_y}{\partial t_e} + \Omega_e i_x + R_y i_y + (-e_{wy} + e_{py} + e_{fy}) \quad (9)$$

$$-\frac{\partial e}{\partial t_e} = \frac{1}{C} (\Delta i_x + \Delta i_y) \quad (10)$$

See Fig. 2 for symbols.

Three scale factors relating the hydrodynamic and electronic system

$$K_t = t / t_e \quad (11)$$

$$K_e = \zeta / e \quad (12)$$

$$K_i = W_x / i_x = W_y / i_y \quad (13)$$

Variables in the linearized electronic and hydrodynamic systems, related by the scale factors

$$L_x = \frac{K_i}{K_e K_t}\frac{\Delta x}{\Delta y}\frac{1}{gh} \qquad L_y = \frac{K_i}{K_e K_t}\frac{\Delta y}{\Delta x}\frac{1}{gh} \tag{14}$$

$$R_x = \frac{K_i}{K_e}\frac{\Delta x}{\Delta y}\frac{r}{gh^2} \qquad R_y = \frac{K_i}{K_e}\frac{\Delta y}{\Delta x}\frac{r}{gh^2} \tag{15}$$

$$\Omega_e = \frac{K_i}{K_e}\frac{\Omega}{gh} \tag{16}$$

$$C = \frac{K_e}{K_i K_t}\Delta x \cdot \Delta y \tag{17}$$

$$Z_{sx} = \frac{K_i}{K_e}\frac{1}{\Delta y}\frac{1}{\sqrt{gh}}\sqrt{\frac{r}{h}\frac{T_e}{j2\pi K_t}+1} \qquad Z_{sy} = \frac{K_i}{K_e}\frac{1}{\Delta x}\frac{1}{\sqrt{gh}}\sqrt{\frac{r}{h}\frac{T_e}{j2\pi K_t}+1} \tag{18}$$

$$e_{wx} = \frac{1}{K_e}\Delta x \frac{1}{\rho g h}\tau_{ax} \qquad e_{wy} = \frac{1}{K_e}\Delta y \frac{1}{\rho g h}\tau_{ay} \tag{19}$$

$$e_{px} = \frac{1}{K_e}\Delta x \frac{1}{\rho g}\frac{\partial p_a}{\partial x} \qquad e_{py} = \frac{1}{K_e}\Delta y \frac{1}{\rho g}\frac{\partial p_a}{\partial y} \tag{20}$$

$$e_{ex} = \frac{1}{K_e}\Delta x \frac{\partial S_o}{\partial x} \qquad e_{ey} = \frac{1}{K_e}\Delta y \frac{\partial S_o}{\partial y} \tag{21}$$

Note: C is independent of h.
L is independent of $\Delta x/\Delta y$, if $\Delta x = \Delta y$.
K_e/K_i can be chosen arbitrarily without changing C or L, if $K_e/K_i K_t$ or $K_i/K_e K_t$ is kept constant.
Terms in the square root of Equation (18) are practically unity for most cases.

Estimation of geostrophic surface wind from an atmospheric pressure field

$$u_a = -\beta \frac{1}{\rho_a}\frac{1}{2\omega_E \sin\phi}\left(\frac{\partial p}{\partial x}\sin\delta + \frac{\partial p}{\partial y}\cos\delta\right) \tag{22}$$

$$v_a = \beta \frac{1}{\rho_a}\frac{1}{2\omega_E \sin\phi}\left(\frac{\partial p}{\partial x}\cos\delta - \frac{\partial p}{\partial y}\sin\delta\right) \tag{23}$$

Wind stress represented by Equations (22) and (23)

$$\tau_{ax} = -\frac{k}{\rho_a}\left(\frac{\beta}{2\omega_E \sin\phi}\right)^2\left(\frac{\partial p}{\partial x}\sin\delta + \frac{\partial p}{\partial y}\cos\delta\right)\sqrt{\left(\frac{\partial p}{\partial x}\right)^2+\left(\frac{\partial p}{\partial y}\right)^2} \tag{24}$$

$$\tau_{ay} = \frac{k}{\rho_a}\left(\frac{\beta}{2\omega_E \sin\phi}\right)^2\left(\frac{\partial p}{\partial x}\cos\delta - \frac{\partial p}{\partial y}\sin\delta\right)\sqrt{\left(\frac{\partial p}{\partial x}\right)^2+\left(\frac{\partial p}{\partial y}\right)^2} \tag{25}$$

Resultant of the wind and pressure disturbances within a grid

$$e_{wx}+e_{px} = -\frac{\Delta x}{K_e \rho g}\left[\frac{k}{h\rho_a}\left(\frac{\beta}{2\omega_E \sin\phi}\right)^2\left(\frac{\partial p}{\partial x}\sin\delta + \frac{\partial p}{\partial y}\cos\delta\right)\sqrt{\left(\frac{\partial p}{\partial x}\right)^2+\left(\frac{\partial p}{\partial y}\right)^2} + \frac{\partial p}{\partial x}\right] \tag{26}$$

$$e_{wy}+e_{py} = \frac{\Delta y}{K_e \rho g}\left[\frac{k}{h\rho_a}\left(\frac{\beta}{2\omega_E \sin\phi}\right)^2\left(\frac{\partial p}{\partial x}\cos\delta - \frac{\partial p}{\partial y}\sin\delta\right)\sqrt{\left(\frac{\partial p}{\partial x}\right)^2+\left(\frac{\partial p}{\partial y}\right)^2} + \frac{\partial p}{\partial y}\right] \tag{27}$$

4. EXAMPLE OF THE MODEL PARAMETERS

As an example, values of parameters for a 330-grid model of the seas around the British Isles are shown here.

The grids of the electronic sea model has been chosen as

$$\Delta x = \Delta y = 50 \text{ Km} \tag{28}$$

so that they match with the 100Km-grid numerical model designed for weather forecasting by the Meteorological Office, as shown in Fig. 4. A single meteorological data is available for every four sea grids.

The three scale factors have been chosen as follows:

$$K_t = 3.60 \times 10^7 \tag{29}$$

$$K_i = 3.60 \times 10^{16} \quad \text{cm}^3\ \text{s}^{-1}\ \text{A}^{-1} \tag{30}$$

$$K_e = 10^3 \quad \text{cm V}^{-1} \tag{31}$$

Examples of the relationship between time in the sea and time in the model are shown in Table 1.

Table 1. Examples of time in the sea and time in the model

t	t_e	$1/t_e$
1 h	0.10 ms	10.00 KHz
6 h	0.60 ms	1.66 KHz
12 h	1.20 ms	0.833 KHz
1 day	2.40 ms	0.416 KHz
6 days	14.40 ms	69.44 Hz
1 year	876.00 ms	1.141 Hz

From Equation (17)

$$C = 19290 \text{ PF} \tag{32}$$

Examples of the values of other parameters related with water depth and/or latitude are shown in Table 2.

Table 2. Example of model-parameter values

h (m)	9.7	21.6	46.0	100	211
L (H)	1.076	0.497	0.227	0.107	0.463
R *(KΩ)	9.95	1.95	0.413	0.090	0.022
Ω_e **(KΩ)	2.45	1.10	0.500	0.240	0.115

* For $r = 0.24$ cm s^{-1} ** For $\theta = 60^\circ$

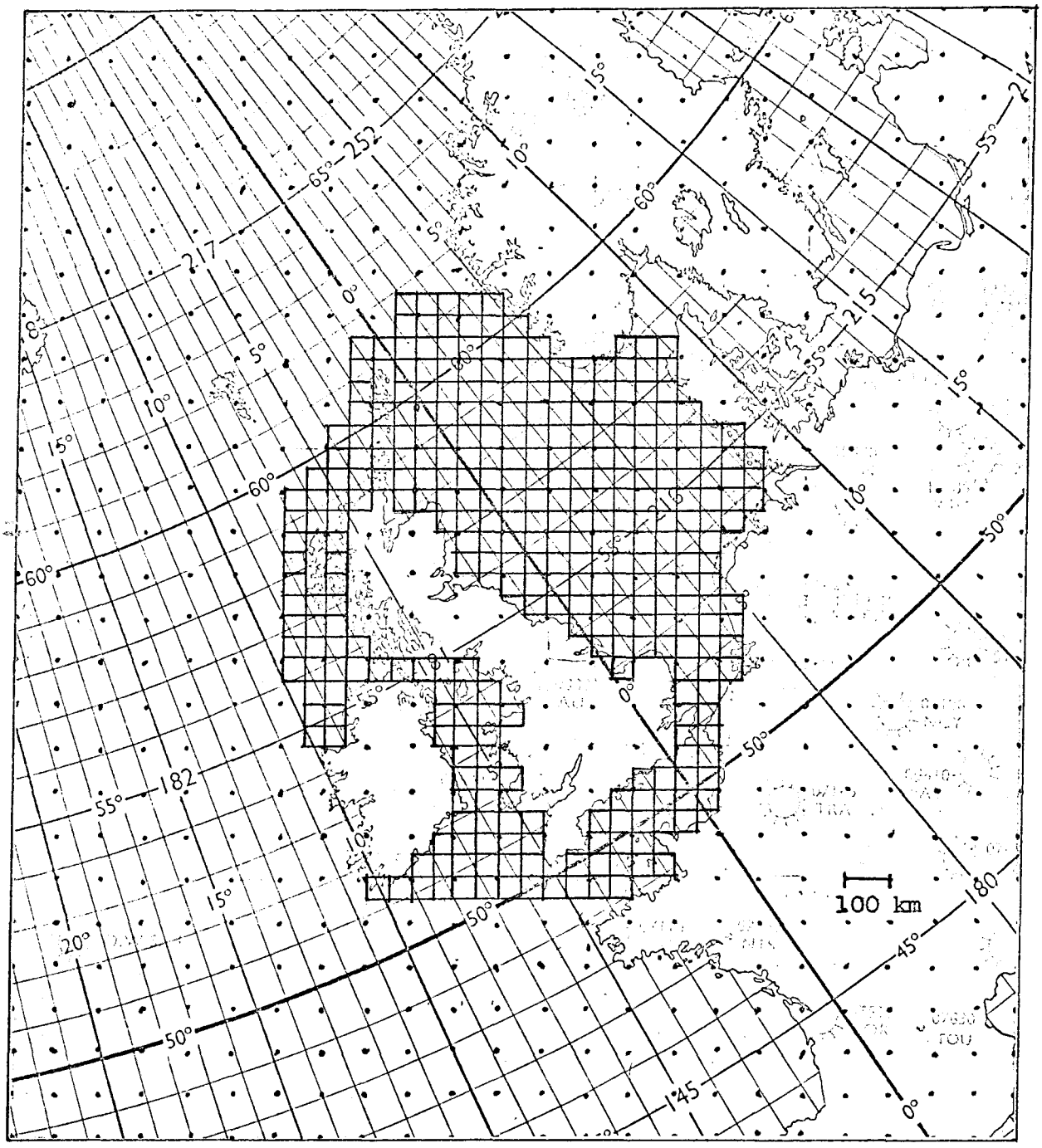

Fig. 4. Example of the arrangement of a 330-grid electronic sea model for the seas around the British Isles.
The sea grids are designed to match with a meteorological grid scheme used for numerical forecasting by the Meteorological Office.
Four sea grids correspond to one meteorological grid.

5. FUNDAMENTAL DESIGN

The MAIN NETWORK consists of a number of grid cards and a matrix socket board with a floating dc-power supply.

Each grid card has an electronic circuit whose principle is shown in Fig. 2. The physical and electronic specifications for the input and output of all the grid cards (including non-linear versions, if made) are uniform so that a combined use of different types of grids on a common matrix socket board is possible.

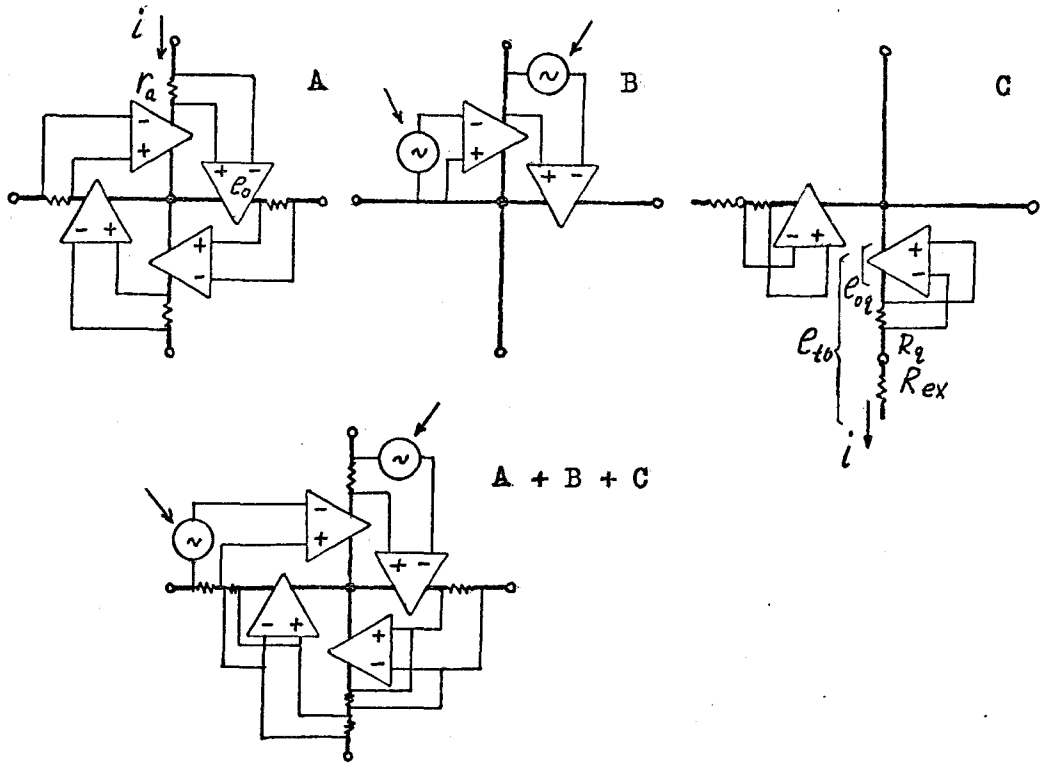

Fig. 5. Schematic diagram of a grid card by which three types of operation are carried out simultaneously.
A: Coriolis force B: All external forces
C: Cancellation of excess resistances

Fig. 5 shows a schematic diagram of the circuit for a single grid card (the inductors and the capacitor are omitted from the figure). This consists of four units of operational amplifiers (OA) with a simple resistance network and two opto-electronic couplers, and carries out three types of operation simultaneously:-

(A) Representation of the Coriolis force

Fig. 5(A) shows the essential part of the circuit for this purpose. A current, i, on each arm is sampled by a current-sampling resistor, r_a, as a voltage, $r_a i$, and this appears on the output of the OA in the adjacent arm, as

$$e_o = A_v r_a i \tag{33}$$

where A_v is the voltage gain of OA. In order to satisfy Equation (16)

$$A_v r_a = \Omega_e / 2 \tag{34}$$

Since the differential voltage across r_a is fed into each OA, its output voltage is independent of the absolute potential at r_a.

(B) Representation of all the external forces

Fig. 5(B) shows the essential part of the circuit for this purpose. Only two OAs in the x and y components are used, since it is enough to represent external forces by those acting between two adjacent grid centres in each component. An opto-electronic coupler is connected to the input of each OA so that the input terminals for the external-force data are electrically isolated from the floating network.

(C) Cancellation of excess resistances in the circuit

Fig. 5(C) shows the essential part of the circuit for this purpose. Again only two OAs are used, due to a similar reason th that for the previous circuit. A current, i, along an arm is sampled by a current-sampling resistor, R_q, as a voltage, $R_q i$, and this is fed into the OA in the arm itself so that the output voltage of the OA is

$$e_{oq} = -A_{rc} R_q i \tag{35}$$

where A_{rc} is the voltage gain and the minus sign shows that e_{oq} and i are in antiphase. e_{oq} is not affected by the absolute potential at R_q, because of the differential input of the OA. If any external resistance, R_{ex}, exists in the arm, the total voltage along the arm is

$$e_{to} = [R_{ex} + R_q (1 - A_{vc})] i \tag{36}$$

Therefore the total resistance along the arm appears as

$$R_{to} \equiv e_{to}/i = R_{ex} + (1 - A_{vc}) R_q \tag{37}$$

Concequently the total resistance can be chosen arbitrarily down to zero, inspite of the existance of R_{ex}, by adjusting A_{vc} and R_q.

R_{ex} could be any resistance between two adjacent grid centres, e.g. the resistance of an inductor, the output resistance of the OA itself, another current measuring resistor. This technique not only extends the range of realization of R (in Equation 15), but makes the design of other parts much easier.

Fig. 5(A+B+C) shows the combined circuit of the above three types of circuit.

6. OPTO-ELECTRONIC COUPLING

6.1 Temparature stabilization

Temperature stabilization of opto-electronic couplers has to be considered separately from those of other components which have little problems.

Generally an opto-electronic coupler in question consists of a Ga-As light-emitting diode whose light-emitting efficiency decreases with temperature, and a silicon photo-transistor whose opto-electronic sensitivity increases with temperature. Since manufacturing deviations of these characteristics are quite widely spread, the combined temperature coefficient of each cpupler also varies quite widely (either positive or negative).

The characteristics of an opto-electronic coupler are not only affected by ambient temperature but by heat generated internally, particularly by the light-emitting diode which has to be driven with a relatively high continuous current in this application.

The use of a feedback circuit, for temperature stabilization, from an electrically floating circuit to a non-floating circuit requires extra components which are comparable to the original circuit components.

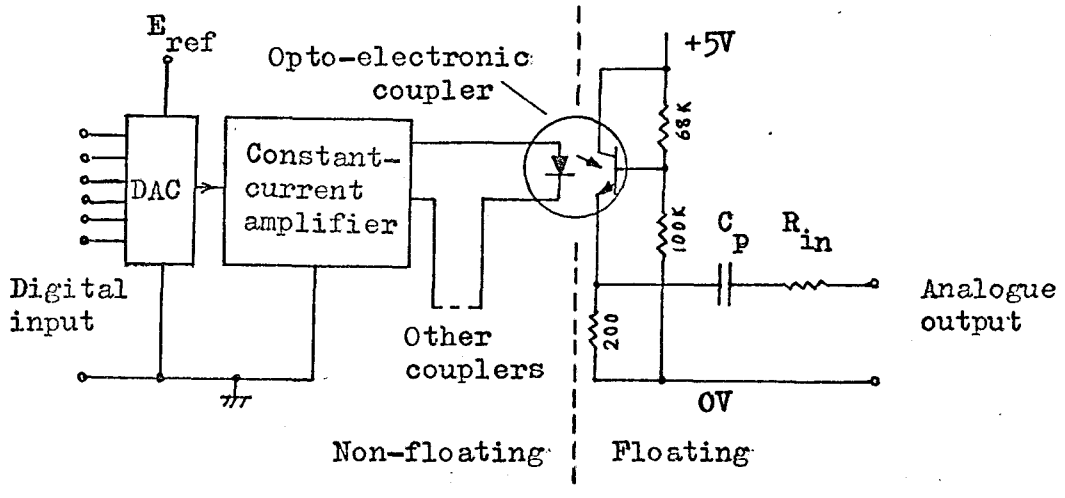

Fig. 6. Schematic diagram of an opto-electronic coupler and related parts.

Fig. 6 shows a schematic diagram of an opto-electronic coupler and related parts. The light-emitting diode of the coupler is driven by a constant-current amplifier (its output current is proportional to its input voltage but is independent of a load connected to the output) whose input signal is supplied from a digital-to-analogue converter (DAC).

Temperature effect of an opto-electronic coupler appears, at its output, as a signal-sensitivity change (ac) and an output-level change (dc). The method of compensation for this effect, applied to the present design, is as follows:-

The output signal of the DAC is a function of digital input and a reference voltage, E_{ref}. If E_{ref} is controlled (manually or automatically) so that the sensitivity change of the coupler due to temperature is compensated, the over-all signal-gain from the digital input to the output of the photo-transistor becomes temperature independent. In order to eliminate the output-level change (dc) due to temperature, a simple high-pass filter consisting of C_p and R_{in} is added, where R_{in} is one of input resistors of the following circuit. The time constant of C_pR_{in} can be chosen easily as more than 1 sec, which is equivalent to more than 1 year in real time, so that the frequancy range of real phnomenon is not affected. Note C_p is the only extra component involved.

In order to design a circuit (could be a single potentiometer) to control E_{ref} for temperature compensation, three types of data are required:

(1) Range and speed of ambient temperature change

Temperature inside the cabinet (152 x 68 x 64 cm^3) which contains all grid cards including couplers in question, and the room temperature (IOS Main Building, Room 6, Wormley, Surrey) were recorded continuously, during a few sampled periods in different seasons including a season in which the room was heated. Daily temperature variation inside the cabinet remains whithin $\pm$ 1.5°C, and seasonal variations of daily-mean temperature remains within 20°C $\pm$ 7°C. The speed of temperature change inside the cabinet is less than 1°C/h in normal operating conditions.

(2) Time constant of temperature change of the couplers

One of the opto-electronic couplers mounted on a standard grid card was chosen as a sample. The temperature change was detected by the collector current of its photo-transistor, and was recorded by a XT plotter. The sample was heated slightly above room temperature, and then released in free air in the room. The time from release to the time taken for the current value to reduce to 0.368 of the value at the instant of release was measured, this being regarded as the thermal time-constant of this type of coupler. The value is 91.0sec.

(3) Temperature coefficient of individual couplers

The full number of couplers, Type TIL-112, were tested by a test curcuit shown in Appendix 2 with a standard input current (1 kHz sine wave of 4 mA peak-to-peak, superimposed on 10 mA dc), at temperature of 30°C and 20°C respectively. The ac compoenent of the output voltage at the emitter of the photo-transistor of each coupler was measured, as E_{30} and E_{20}. Then $(E_{20} - E_{30})/E_{20} \cdot 10°C$ is regarded as the temperature coefficient of the coupler. The value of E_{20} is used as an indicator of its individual sensitivity. All the couplers were divided into 5 groups depending on the temperature coefficients as shown, together with the number of couplers in each group, in Table 3. Some couplers (Groups H and L) are outside the specified ranges. Examples of the temperature effect of couplers are shown in Appendix 1.

Table 3. Temperature coefficient of opto-electronic couplers, Type TIL-112, and numbers in each group.

Group	Temperature coefficient (%/°C)	Number of couplers
H	+0.60	2
a	+0.50 to +0.59	17
b	+0.30 +0.49	174
c	+0.29 +0.10	316
d	+0.09 -0.09	127
e	-0.10 -0.29	22
L	-0.30	6
Abnormal		7
	Total	665

From (2) we understand that ambient temperature changes faster than say 10 sec, even if they exist, would not affect normal operations of the grid cards. From (1) and (3) we also understand that maximum temperature effect on the couplers with no compensation would be between +4.2% and -2.1%, if the cards are calibrated at 20°C. The maximum temperature effect would be between +0.90% and -0.45%, for the same grid cards, if E_{ref} for each group of couplers (5 groups in all) is individually adjusted for the daily-mean temperature of a particular period (e.g. a season).

In conclusion, the simplest method of temperature compensation for the couplers is to provide five different values of E_{ref}, which can be adjusted individually, and to adjust them seasonally. It is possible to design a simple circuit to carry out this operation automatically.

6.2 Sensitivity

The sensitivity of opto-electronic couplers is indicated generally by their current transfer ratio. This for the chosen type of couplers, TIL-112, is read on the published data sheet as 2% minimum and 20% typical (at LED forward current = 10 mA, and transistor collector-emitter voltage = 5.0V. These are rather poor absolute values and manufacturing deviation; this type of coupler having been chosen 2 years ago because of the lowest price at the time. An advance of opto-electronic industry has made a similar type of coupler having more than 100% current transfer ratio available at the same or even lower price now.

A feedback circuit applied to the photo-transistor of an opto-electronic coupler, as shown in Fig. 6, which is intended to improve its frequency range also has an effect of reducing the variation of the sensitivity from device to device, although this has to be compromized with the reduction of the sensitivity.

As described in 4.1.2(3), the sensitivity of this type of coupler in the full purchased quantity, excluding a few abnomal deviced, was measured individually at 20°C by the circuit described in Appendix 2. Table 4 shows the results.

Table 4. Number of opto-electronic couplers, Type TIL-112, against the relative sensitivity. Measured at 20°C by the circuit shown in Appendix 2.

Relative sensitivity	Number
10 to 19	69
20 29	184
30 39	149
40 49	119
50 59	72
60 69	35
70 79	17
80 89	7
90 99	1
100	1
Total	655

In the present design, the coupler and grid cards have been combined so that the order of the sensitivity of couplers is inversely proportional to the serial number of cards, within the same temperature-coefficient group shown in Table 3. This arrangement is convenient for selecting the cards for the topography to be modelled, because generally a wide-amplitude operation is required for a grid representing shallow water depth.

7. ELECTRONIC DESIGN

Fig. 7 shows the circuit diagram of a single grid card. Each of four arms, ON, OE, OS, OW, has potentiomater r_a by which Ω_e is set in the grid. Each of the arms OS and OW has a fixed resistor R_q by which the fixed value of e_{oq} (in Equation 35) is obtained; an arbitary value of R_{to} (in Equation 37) is obtained by adjusting another potentiometer r_v (in arm OE or OS). Each OA in arms ON and OE has an opto-electronic coupler input, and its gain is controlled by a potentiometer r_p. The value of r_p has been chosen much higher than the fixed resistance R_p and R_p' so that the adjustment of r_p does not affect the rest of the input circuit. The opto-electronic input is coupled to the OA by a capacitor, C_p for temperature stability (see 4.1.2), and C_p is used for balancing the differential input impedance. Each part of resistances in the differential input has a fixed value, but this is matched within ± 0.2% (see Appendix 6).

Each of arms ON and OW has an inductor, L (see page 21), and a current-measuring resistor R_i; the voltage between terminals N-N_i or W-W_i is proportional to the current along each arm, and from this voltage, u or v (see Chapter 2) is obtained. A capacitance, C, specified by Equation (17) is connected between the grid centre to earth.

Two dual IC packages, Type 747C, are used for the two OAs in each grid card; one package for the OAs in arms ON and OE, and the other package for arms OS and OW. Since the latter requires better high-frequency characteristics than the former, this combination helps for efficient use of ICs. Note the manufacturing deviation of high-frequency characteristics of ICs is rather large (see Appendix 3).

All the OAs and transistors (not LEDs) in the opto-electronic couplers are operated by a single floating dc-power supply (see 4.2) through a stabilized voltage divider.

The grid cards should be designed so that an arbitrary topography (not a particular sea) can be modelled. In practice, an applicable water-depth range is assumed between 10m and 211m approximately for the present grid cards (linear version). This will cover most seas where storm surges are interesing and tides are significant for practical applications. In order to treat water-depth less than 10m, grid cards with non-linear characteristics will be necessary. For the convenience of design of electronic components, in fact mainly variable inductors, grid cards (linear version) are divided into five groups depending on water depth as shown in the first and second rows of Table 5. The designed values of the components are shown in the same table.

The variation of values in the groups is due to the variation of range of W, ξ, r, Ω of the hydrodynamic system as well as water depth h itself. The range of these factors are taken from observational data, assuming the sea is in the latitude between 70°S and 70°N approximately. Economical operating ranges of electronic components, e.g. noise level, maximum amplitudes, are also taken into account.

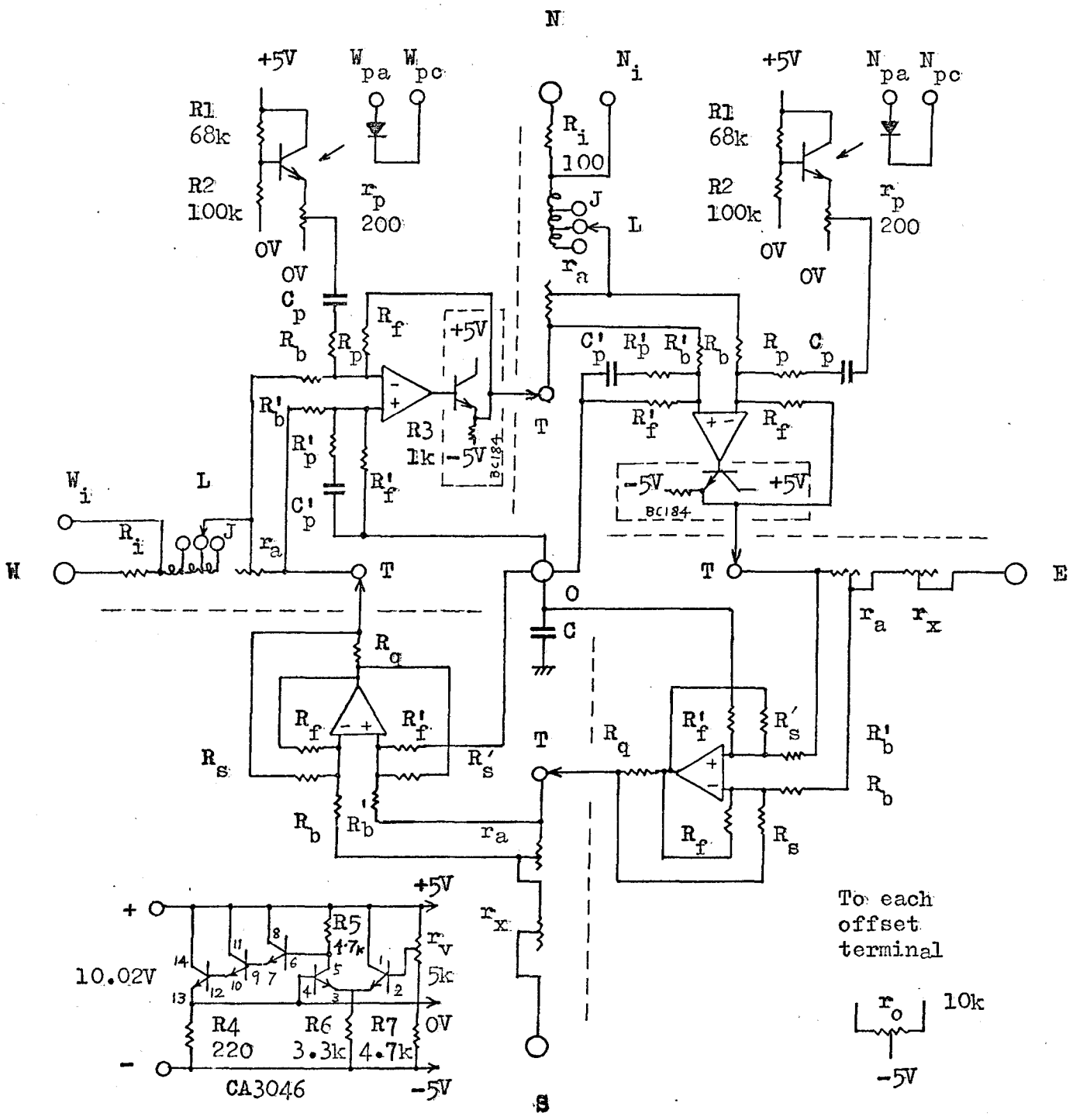

Fig. 7. Circuit diagram of a grid card (linear version). The power supply lines and the offset terminal lines are not shown. Two transistors in the dotted frames are used for grid cards representing deep water only. See Table 5 for components.

Table 5. Values of model parameters and components for grid cards

Grid card Nos.			1001 to 1038	2001 to 2085	3001 to 3105	4001 to 4060	5001 to 5040
h		m	9.7 21.6	21.2 47.0	46.0 100	99.9 170	169 211
W_{max}		$cm^3 s^{-1}$	1.0 x 10	3.0 x 10	7.5 x 10	7.5 x 10	7.5 x 10
i_{max}		mA	0.029	0.086	0.215	0.215	0.215
ζ_{max}		cm	300	150	75	75	75
$e_{\zeta max}$		mV	300	150	75	75	75
$\Omega_e/2$ $\theta=60°$		Ω	2.45k 1.1k	1.1k 500	500 237	240 140	140 115
R		Ω	10k 1.95k	2.0k 400	413 89	90	22
R_L		Ω	314 237	129 92.4	58.4 44.4	28.7	21.8
R_i		Ω	100				
NW	e_p	mV	170	120	60		25
	$r_{p\,max}$	Ω	200				
	R_p	Ω	100k				
	R_f	Ω	330k				
	A_p	-	3.3				
	$e_p A_p$	mV	560	396	198	82	
	C_p	μF	40				
	$r_{p\,max}/R_p$	%	0.2				
	R_b	Ω	100k				
	A_r	-	3.3				
	$r_{a\,max}$	Ω	1k	500	200	100	100
	$\Omega_e/2_{max}$	Ω	2.75k	1.38k	550	2.75	
	$r_{a\,max}/R_b$	%	2.75	1.38	0.55	0.28	
	Z_o @ 1KHz	Ω	5				
SE	R_g	Ω	1.2k	680	330	180	120
	R_s	Ω	33k				
	R_f	Ω	100k				
	A_s	-	3.0				
	R_g/R_s	%	3.6	2.0	1.0	0.5	0.4
	R_N	Ω	2.4k	1.36k	660	360	240
	R_b	Ω	39k				
	A_v	-	2.56				
	r_a	Ω	1k	500	200	100	100
	$\Omega_e/2$	Ω	2.56k	1.28k	512	256	
	r_a/R_b	%	2.6	1.3	0.5	0.3	0.3
	$12r_a + R_i + R_L + Z_c$	Ω	2.42k	1.35k	558	329	329
	r_x	Ω	10k	2k	500	100	100

The number of 330 grid cards involving some 15,000 components is too small for making totally integrated circuits economically, though this number is rather large for a laboratory work. Exersizes show that the total cost of components and assembly varies very widely depending on their types, tolerances, and the total quantity purchased and assembled per operation. The present design, which is a hybrid of standard integrated circuits and a few discrete components mounted on a printed circuit board, is an optimum in economy, considering the availability of components in UK in 1972/73; in fact most components had to be imported.

ICs Generally the price of ICs largely depends on the total production quantity of a single type rather than its quality or the degree of complexity of its circuitry. Therefore, one of the most popular type of OAs in ICs, 747C, has been chosen. The high-frequency characteristic required for this purpose was tested for the full quantity of 660 by using a quick test method (see Appendix 3), and the better half is used for the N and W components, and the rest for the E and S components. For the opto-electronic coupler, Type TIL-112, has been chosen being the most inexpensive type at the time of designing. For the stabilized voltage-divider, Type CA-3046 has been chosen again as one of the most inexpensive ICs containing five transistors.

Potentiometers Preset potentiometers in this application require a relatively high stability over a reasonable period. Among many types of cermet potentiometers, Beckman Model 72P has been found as the best value; the lowest price to satisfy the MIL Specifications including temperature stability of 100 ppm/°C, although poor availability in UK which caused the long delay in completion of the work.

Resistors Temperature stability better than 100 ppm/°C and small size less than 10 mm x 2.5 mm ϕ (except for some high resistance) were the first conditions of the choice. The tolerance of resistance values was not tightened (say $\pm$ 2%) so that resistors were available inexpensively. The purchased resistors were divided into $\pm$ 0.2% intervals of each nominal resistance value by a digital ohm-meter. The total cost including the cost of dividing is still far less than the price of resistors having $\pm$ 0.2% tolerance.

Coupling capacitors The coupling capacitors for this application require about 40 μF, 5V working voltage, and a small physical size. Absolute value of the capacitance is not critical, but matched pairs (say within $\pm$ 0.2%) are required for balancing the differential input of the OAs. Since the initial purpose of using the capacitors is to eliminate the temperature effect of the transistor in each opto-electronic coupler, the leakage current of the capacitors should be independent of temperature, or the current should be negligible. Resin-dipped solid-state tantalum capacitors have been chosen, allowing a wide tolerance in capacitoance ($\pm$ 20%). In order to obtain matched pairs, a selection method described in Appendix 4 was used.

Capacitors — Since the capacitance specified by Equation (17) is proportional to the area of a grid ($\Delta x \times \Delta y$), it is not necessary to be varied continiously, but in steps of a reasonably wide range. The combinations of three different values of capacitors, in series and/or parallel, can make 14 different values. For example, by combining three capacitors having the capacitance ratio of 1:2:4, the following ratios can be made:

0.75, 0.85, 1.00, 1.25, 1.50, 1.75, 2.00,
3.00, 3.25, 4.00, 5.00, 5.50, 6.00, 7.00.

Note the cost of three standard capacitors is less than that of a single non-standard capacitor. Standard polystyrene capacitors having capacitances of 15,000 PF, 3,300 PF, and 560 PF (all ± 1%), temperature stability better than ± 100 ppm/°C have been chosen for the present model.

Inductors — Each inductor for this application must be continuously variable in as wide range as possible without changing its Q value. After extensive theoretical and experimental investigations, it was found that the design described in Appendix 6 gives the best results for the purpose; the combination of the types of component is not an intended one by the manufacturer. An example of the variation of an inductor is shown in Fig. 8. The inductors are divided into four groups depending on water-depth ranges applicable. Each inductor has three winding sections with taps. Changing of the taps is carried out by micro sockets on the printed circuit board.

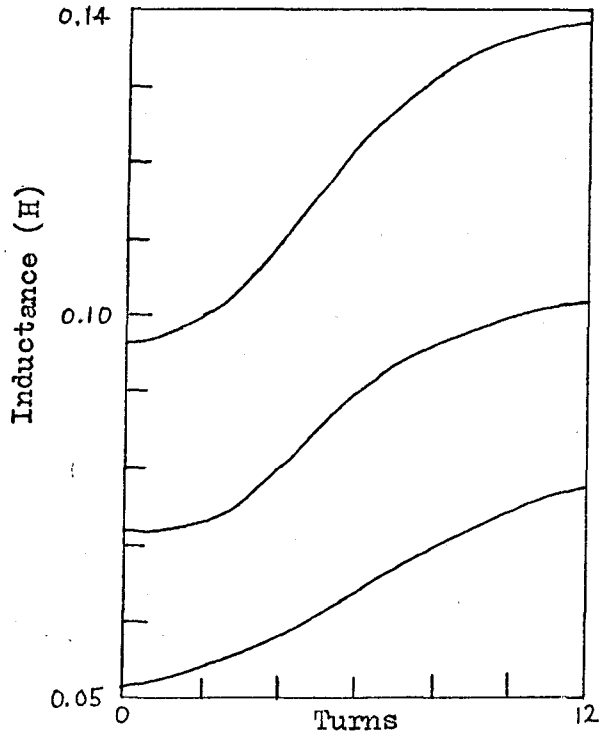

Fig. 8.
Typical characteristics of variable inductors with three winding sections, inductance against turns of the centre core.

A large number of inductors made for the previous model scheme in 1969 have to be used for the present model for economy, although new types of core having smaller physical size and simpler construction are now available. Note the technique described in 4.1.1(C) makes high-quality inductor not very necessary.

8. PHYSICAL DESIGN

Figs. 9 and 10 show the physical design of the grid cards. All the cards have a uniform construction, except for a few extra components for the cards representing deep water. Each card has overall dimensions of 105mm x 65mm x 15mm (highest components). Components are mounted on a single-sided printed circuit board of 1.59 mm epoxy glass with 0.0357mm copper. Components whose height is greater than 6mm are mounted near the centre of the board so that adjacent boards can be overlapped partly and the packing density of the cards in the cabinet is optimized.

Components relating to the four directions, N, E, S, W, are mounted on four symetrical sections of each board which correspond physically to the four directions so that it is easy to remember them. Four potentiometers for preset adjustments which are required only when the card is assembled are mounted near its centre while other potentiometers are near the edges. Four sets of lead and micro socket (external diameter, approximately 1 mm) are used for (1) switching the polarity of the Coriolis parameter, and (2) calibrating model parameters by connecting the leads and sockets with the grid-card calibrator (5.1). Three capacitors specified by Equation (17) are mounted in a part of the board where it is easy to replace the components.

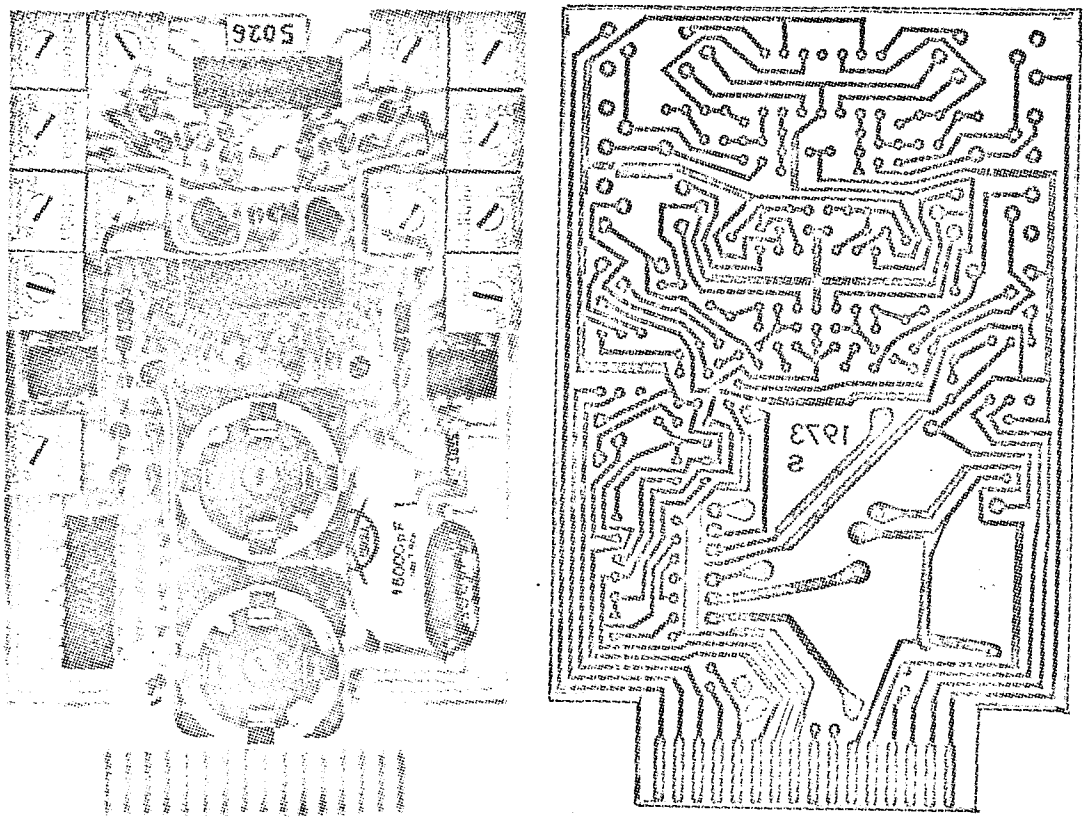

Fig. 9. Physical design of grid cards, linear version (actual size). 330 cards in all have been made. Two sets of a transistor and a resistor are used only for card Nos. 4001 to 4060 and 5001 to 5040.

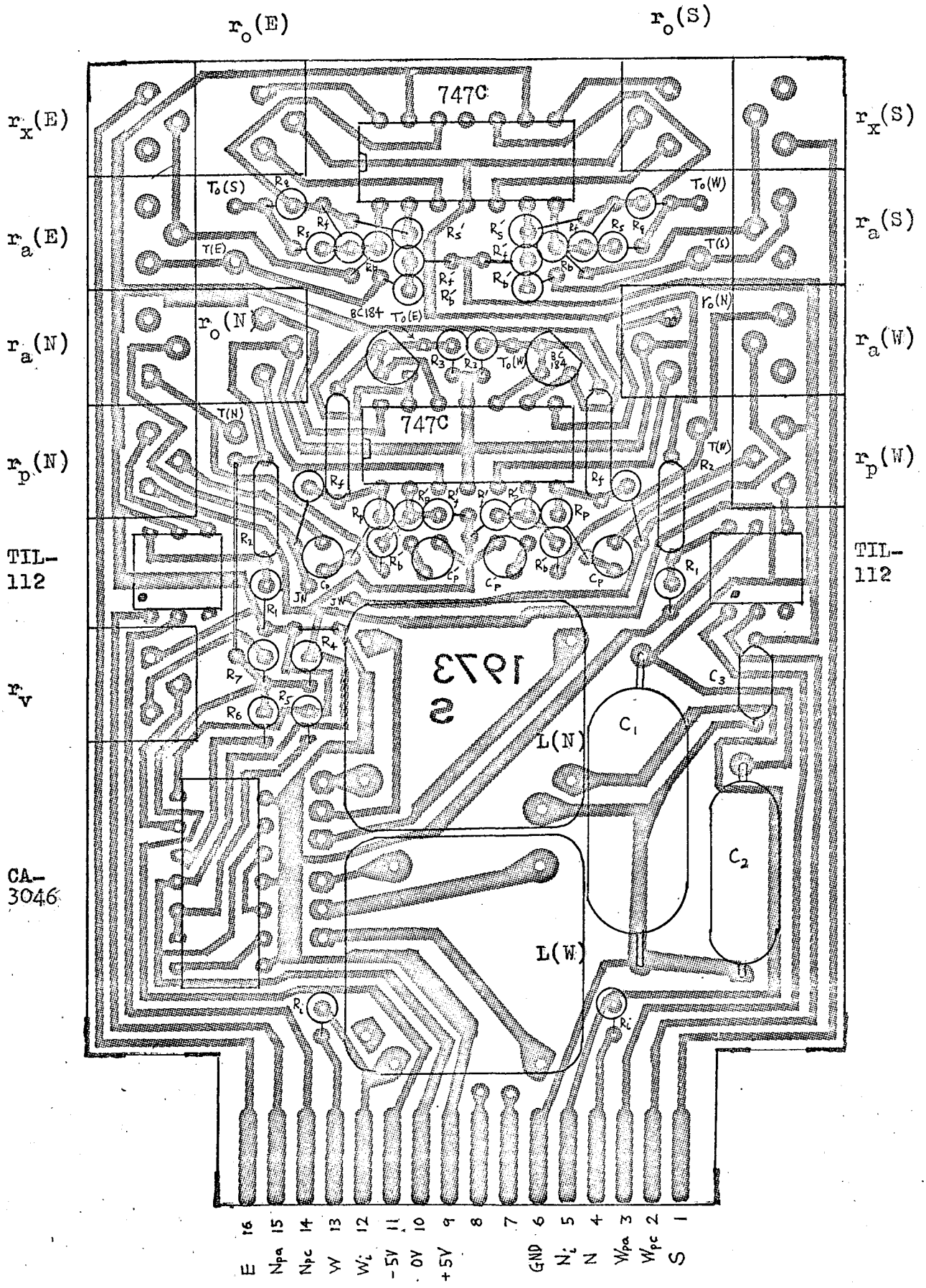

Fig. 10. Physical design of grid cards, linear version (scale x2).

9. FLOATING DC-POWER SUPPLY

The centre of each grid (O in Fig. 7) is taken as the common conductor of all the active components within the grid card, except for the LEDs of the opto-electronic couplers. The centre should have an arbitrary electric potential referred to a common conductor (earth) throughout all the grids of the MAIN NETWORK. Consequently each grid has to be driven by a floating dc-power supply.

Among a few possible methods of realising such a power supply, a system consisting of an electrical isolation transformer (operated from an ac power line), a rectifier and a dc voltage stabilizer is considered to be the most efficient one. The transformers for this purpose require a very high degree of electrical isolation (ideally a magnetic coupling only); e.g. more than a few 100 M ohms for dc, and less than a few PF for ac, between the primary line and the secondary output terminals.

Only one type of standard isolation transformer (made in USA) which satisfies our electric specifications, but a high price (£7.00 each approx.) and large physical size, was found at the time of the designing. Therefore, the floating dc-power supply was developed for the purpose. The cost of the designed transformer (including that of assembly, but excluding design) was £2.13 each for the quantity of about 500, and the total cost of the unit including the rectifier and voltage stabilizer was £6.49 per unit in 1971.

Fig. 11 shows the circuit diagram of the floating dc-power supply, where R_S and C_S are the resistance and capacitance by which the quality of this system can be evaluated. Fig. 12 shows a complete unit and components contained in the unit. Details of the physical design are shown in Appendix 5. The screening of windings in this design is achieved by aluminium foil which is manually formed along each winding; however it is now possible to screen the winding by electrically conductive paint which is quick and easy to complate. A summary of the floating dc-power supplu is as follows:

Input	17V rms ± 1%, 50 Hz
Output	10V ± 0.1% dc, 0 to 60 mA
Noise voltage between floating terminals and earth	1 mV peak-to-peak
Capacitance between floating terminals and earth	PF
Resistance between floating terminals and earth	M ohms
Temperature stability (10 to 35°C)	-0.1% of value at 25°C
Transient voltage drift after switch on	Less than 0.05%
Physical dimension, over all	100 mm X 32 mm ø

Fig. 13 shows the arrangement of circuits between a power line and the floating-dc power supply. Fig. 14 shows its stabilities. Every 60 power supply units are mounted on a single frame which has screen ducts for the input lines.

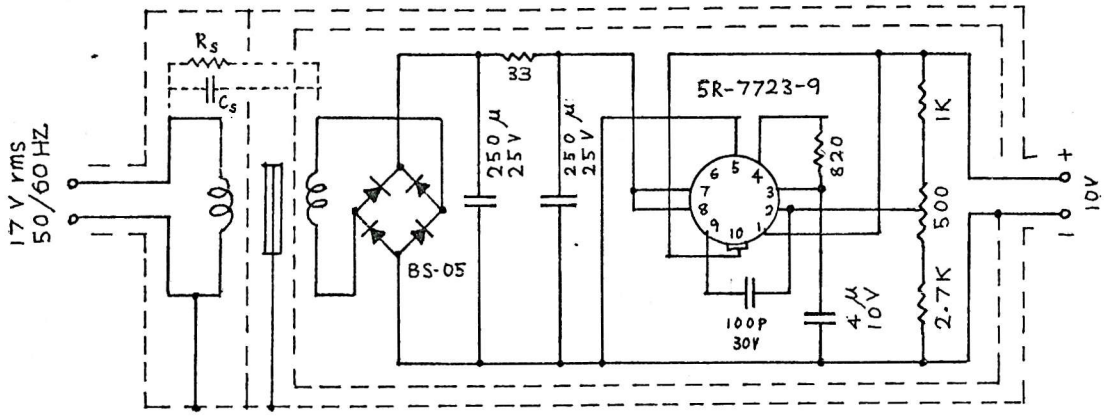

Fig. 11. Circuit diagram of the floating dc-power supply.

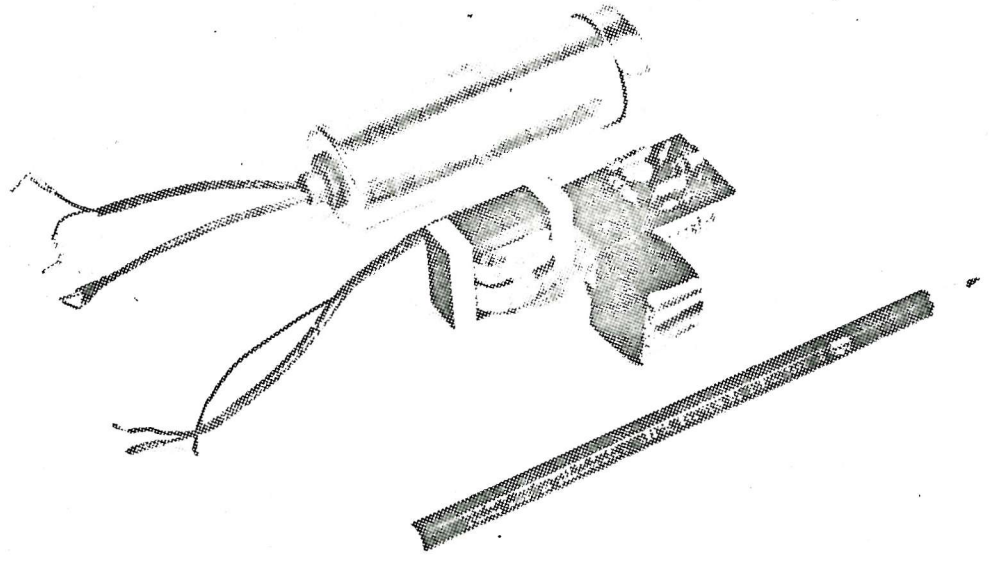

Fig. 12. Floating dc-power supply unit, and its components (from left, the isolation transformer, inner screen, and printed circuit board on which the rectifier and voltage stabilizer are mounted).

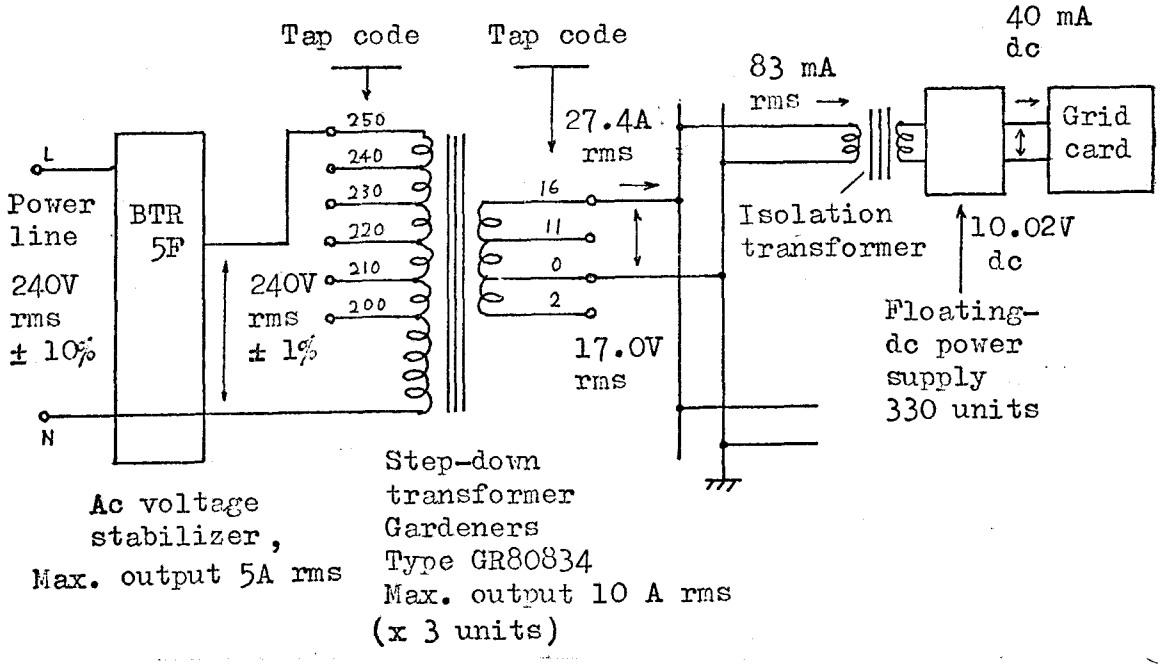

Fig. 13. Arrangement of circuits between a power line and the floating-dc power supply.

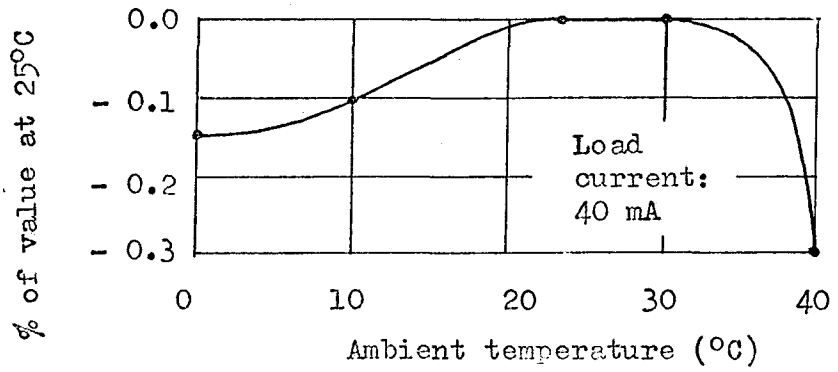

Output voltage change due to ambient temperature

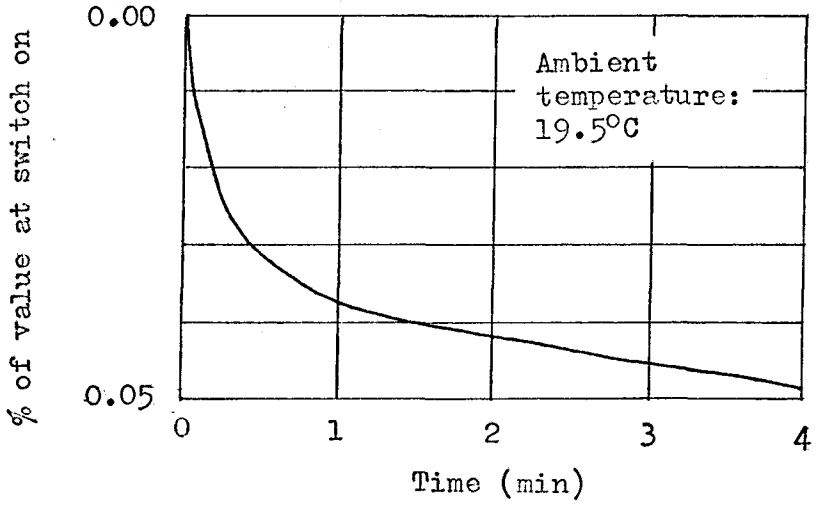

Output voltage change with time after switch on

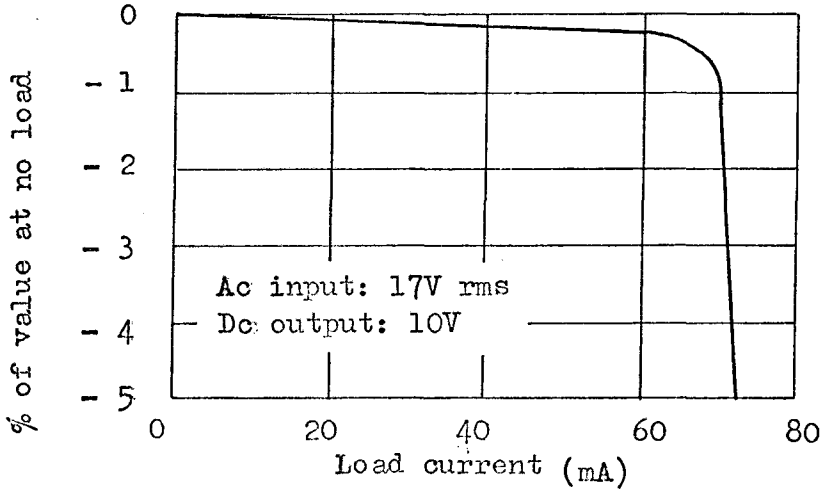

Output voltage change due to load current
(A single grid card requires 40 mA at 10V)

Fig. 14. Stabilities of the floating-dc power supply.

10. PERFORMANCE

The performance of the grid cards can be tested by the grid-card calibrator (5.1) with a few external measuring instruments. the performance has been evaluated by the following factors:-

(1) Setting of the stabilized voltage-divider

By feeding 10.0V dc to the power line of a grid card, the positive and negative outputs of the divider were measured. Potentiometer r_V was adjusted so that the outputs whow +5.00V±0.2% and -5.00V±0.2% respectively. This is satisfactory.

(2) Setting of the offset voltages

Four potentiometers r_o (for N, E, W, S components) were adjusted so that the output level of each OA became OV≅ 1mV. This is satisfactory.

(3) Setting of the Coriolis parameter

By feeding a constant 0.100 mA rms ±0.2% sine-wave current to each unit of N, E, S, W components, its outputs were checked, for waveform, phase relationship between the input and output, and adjustable range of potentiometer r_a. Also by feeding triangular-wave current, the range of linearity of each unit was checked. All of them are satisfactory.

(4) Frequency responce of the Coriolis parameter in the model

By feeding a constant amplitude current having frequency from DC to 20 kHz, with a constant value of Ω_e, the frequency characteristic was measured. Fig. 15 shows a typical result.

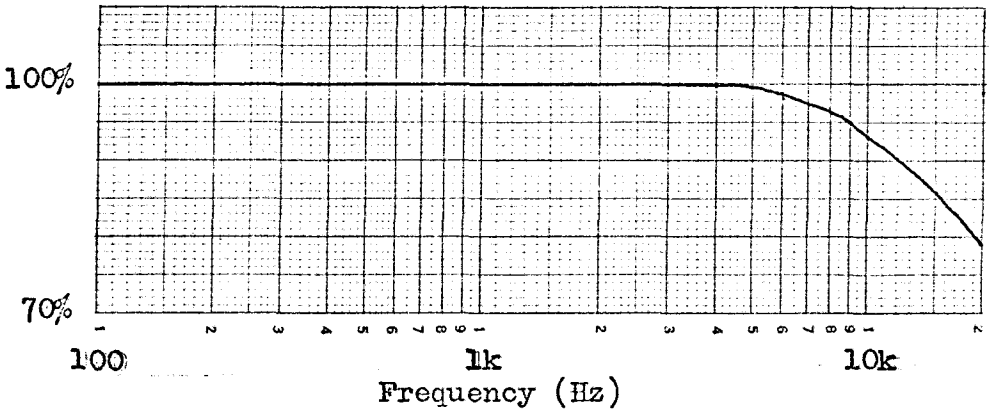

Fig. 15. Frequency responce of the Coriolis parameter in the model, flat from dc.

(5) Setting of the external-force-input gain

The overall gain of the exteral-force input depends on the sensitivity of the coupler used and the setting of potentiometer r_p. This was tested by feeding the standard input signal specified in 3 of Table 6. By feeding a triangular-wave current, the linearity and phase relationship were also tested. These are satisfactory.

(6) Frequency response of the external-force circuit

This response depends on the combined characteristics of an opto-electronic coupler used and OA, mainly the latter. Therefore, the response was measured by using the combinations of three couplers (high, typical and low sensitivity) and two OAs (wide and narrow frequency range). Fig. 16 show the results. Although there is a slight increase of the gain at about 50 kHz when the wide-grequency-range OA is used, a current having this order of frequency does not pass the MAIN NETWORK. The results are satisfactory.

The low end of this frequency response is determined by a CR high-pass filter used at the output of each opto-electronic coupler. The time constant of the filter is from 2.0 sec to 3.5 sec depending on the capacitor used.

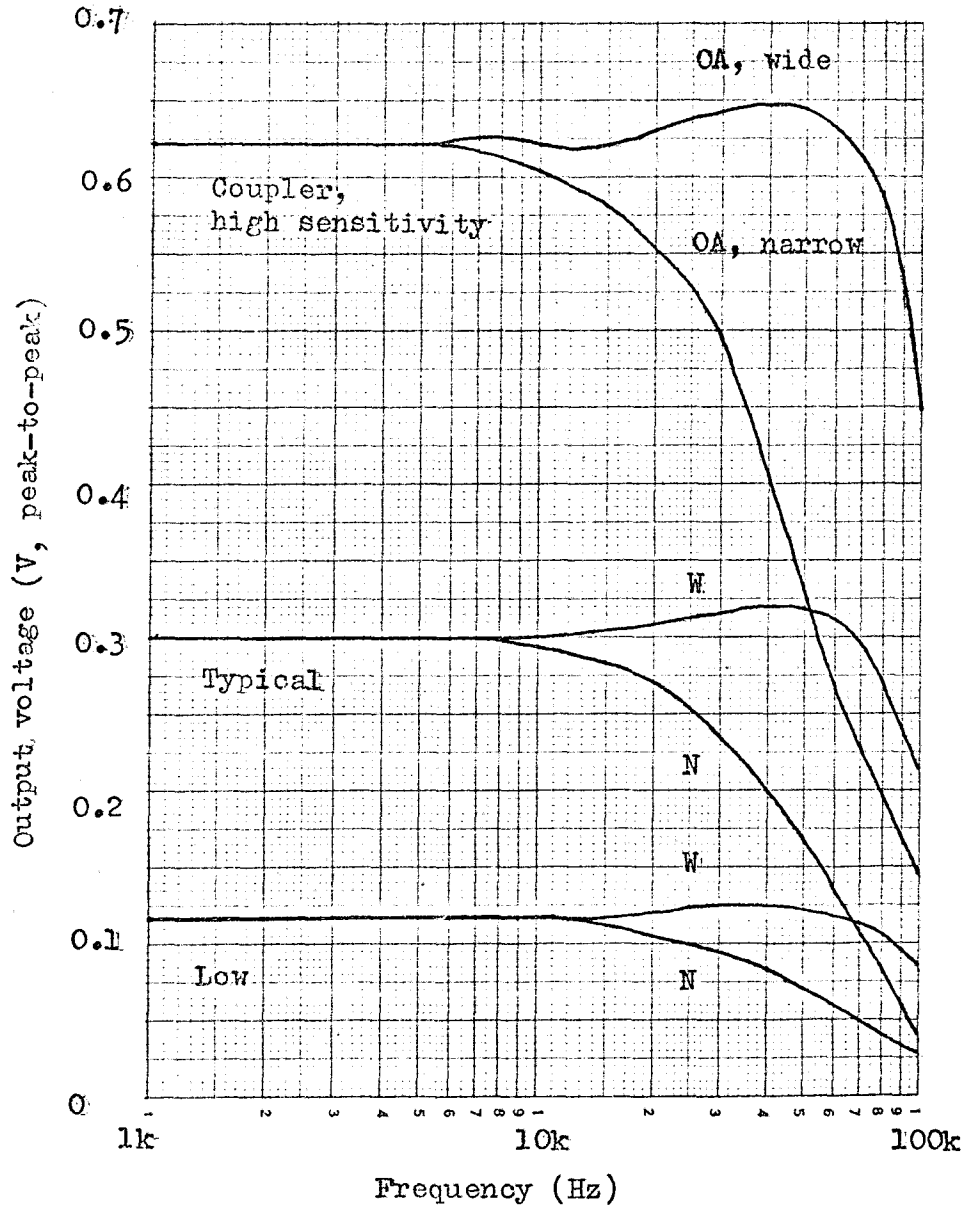

Fig. 16. Frequency responses of the external-force input circuit obtained by combinations of different opto-electronic couplers and OAs.

(7) Setting of excess-resistance cancelation circuit and its frequency responses

The excess-resistance cancelation, expressed by Equations (35) to (37), is based on the assumption that no phase shift occures between the input and output of the OA. A high frequency at which the phse shift is noticeable depends on each OA. Therefore, the test were carried out by using two typical OAs, one is typical of OAs whose frequency range is narrow (N), and the other one is wide (W). The tests were also carried out for five different values of the current-sampling resistor, R_q, shown in Table 5, i.e. 1.2kΩ, 330Ω, 180Ω, and 120Ω which are used for grid card serial Nos. 1---, 2---, 3---, 4--- and 5--- respectively. A constant-amplitude sine-wave current (0.0500 mA peak-to-peak) with various frequensies was used throughout all the tests, and the external resistance was changed adequately.

Fig. 17 shows the result. At low frequency (say below 100Hz), the apparent total resistance, R_{to}, can be set from practically zero to (R_{ex} + Rq) for all the values of R_q. At a frequency higher than say 100 Hz, the flat frequency-range depends on the required value of R_{ex} and OA used. Refering to the set of groups for R_q = 680Ω, for example, an external resistance of 1.5kΩ can be reduced, by OA(W), to 200Ω with a frequency range of dc to 4kHz (resistance rize of +10% at high-frequency end), or by OA(N) to 800Ω with dc to 3kHz. The practical requirement for this set is to reduce the external resistance of 1.5kΩ to 1.0kΩ, for example, i.e. the flat range of the frequency response will be much wider. Note 4kHz in the model corresponds to the period of 2.5h in the sea.

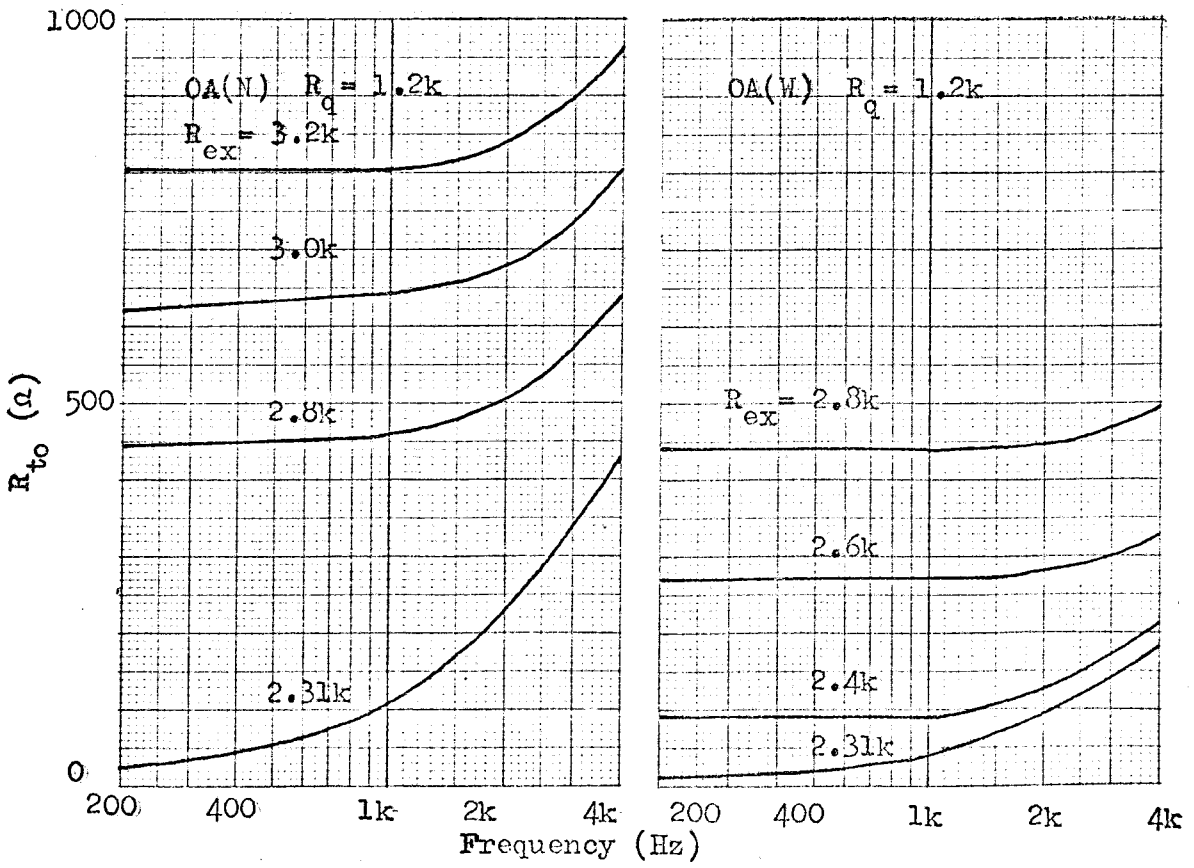

Fig. 17. Frequency responses of the excess-resistance cancelation circuit.

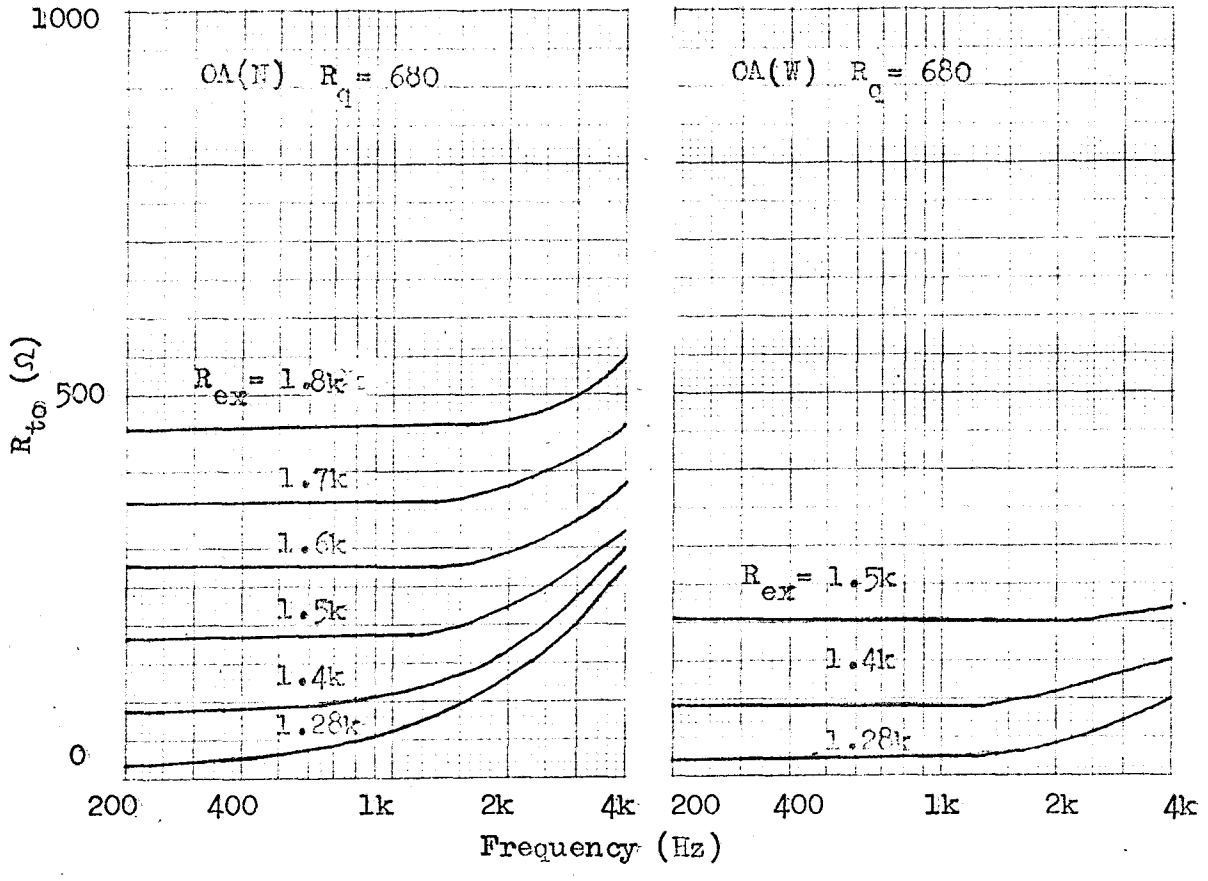
1000
500
0
R_{to} (Ω)
OA(N) R_q = 680
R_{ex} = 1.8k
1.7k
1.6k
1.5k
1.4k
1.28k
OA(W) R_q = 680
R_{ex} = 1.5k
1.41k
1.28k
200
400
1k
2k
4k
Frequency (Hz)

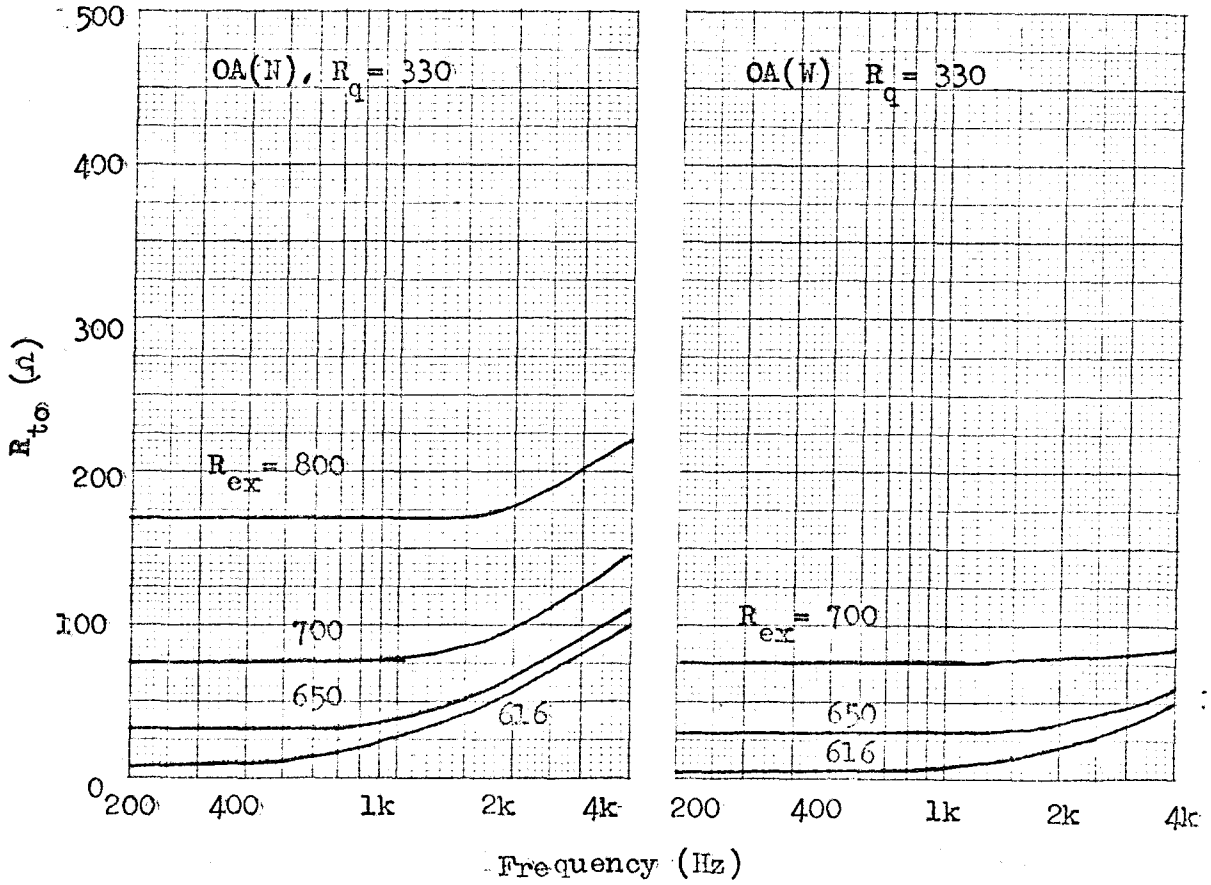
500
400
300
200
100
0
R_{to} (Ω)
OA(N), R_q = 330
R_{ex} = 800
700
650
616
OA(W) R_q = 330
R_{ex} = 700
650
616
200
400
1k
2k
4k
Frequency (Hz)

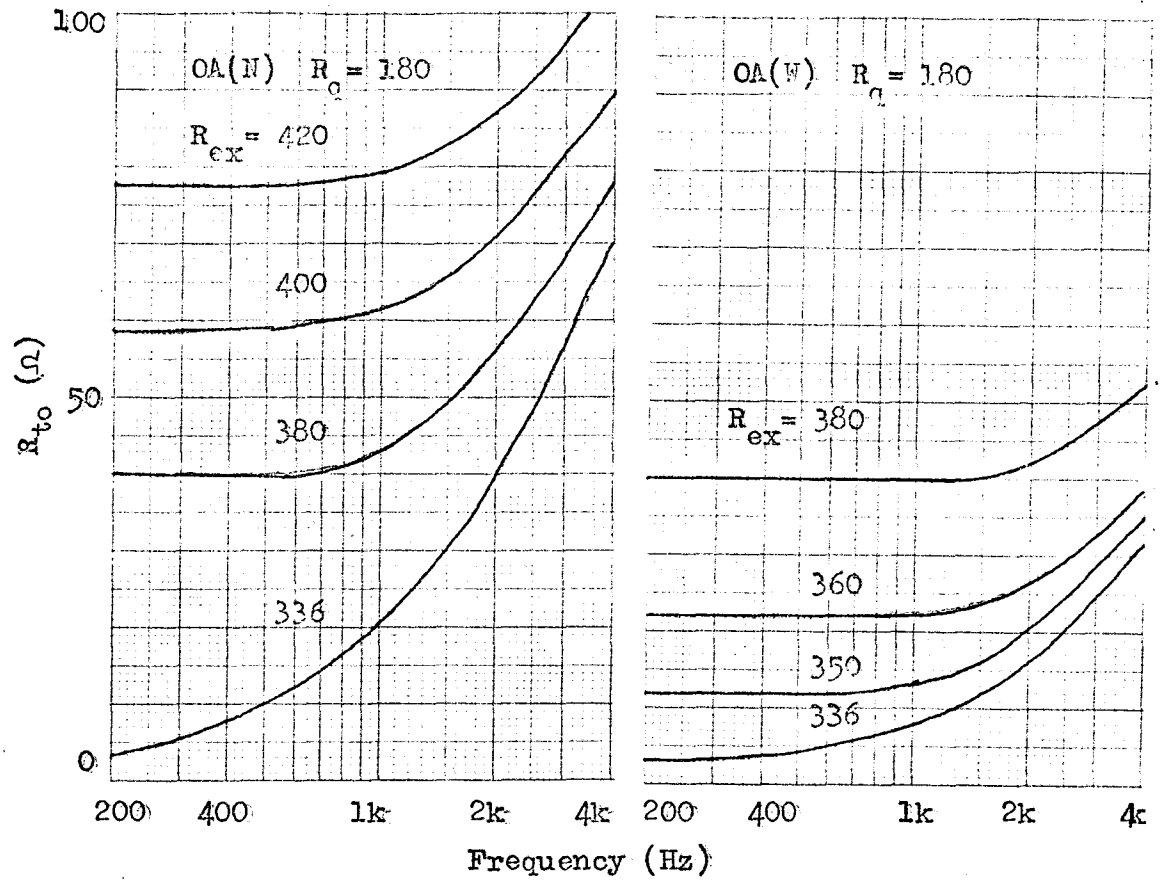
100
50
0
R_{to} (Ω)
OA(N) R_g = 180
R_{ex} = 420
400
380
336
OA(W) R_g = 180
R_{ex} = 380
360
350
336
200
400
1k
2k
4k
Frequency (Hz)

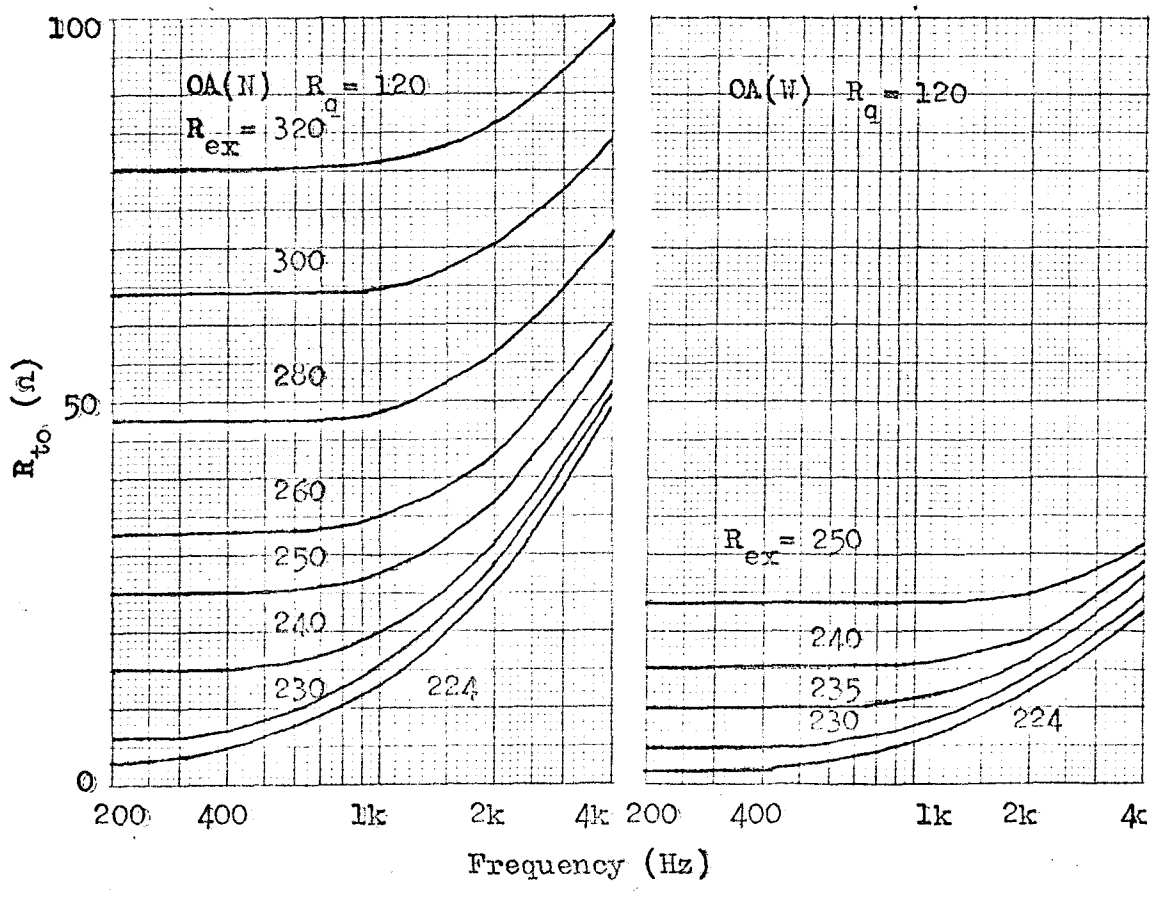
100
50
0
R_{to} (Ω)
OA(N) R_g = 120
R_{ex} = 320
300
280
260
250
240
230
224
OA(W) R_g = 120
R_{ex} = 250
240
235
230
224
200
400
1k
2k
4k
Frequency (Hz)

(8) Impedance between terminal E (or N) and the grid centre

The impedance between terminal E (or N) and the grid centre was measured, while that for terminal W (or S) is given in (7). Fig. 18 shows the result. The impedance in question for grid card Nos. 1--- to 3--- is the output impedance of an OA used itself. This is a few ohms at a low frequency, and increases from a frequency higher than say 1 kHz; 8Ω to 16Ω at 4 kHz depending on the OA. These values are still small enough compared with the value of R shown in Table 2, i.e. 90Ω to 10 kΩ approximately. The impedance for grid card Nos. 4--- and 5--- is that of the OA through an additional transistor. The increase of impedance with frequency is not noticiable at 4 kHz, and its value is 2Ω to 6Ω approximately. This is small enough compared with the value of R which is 90Ω to 20Ω.

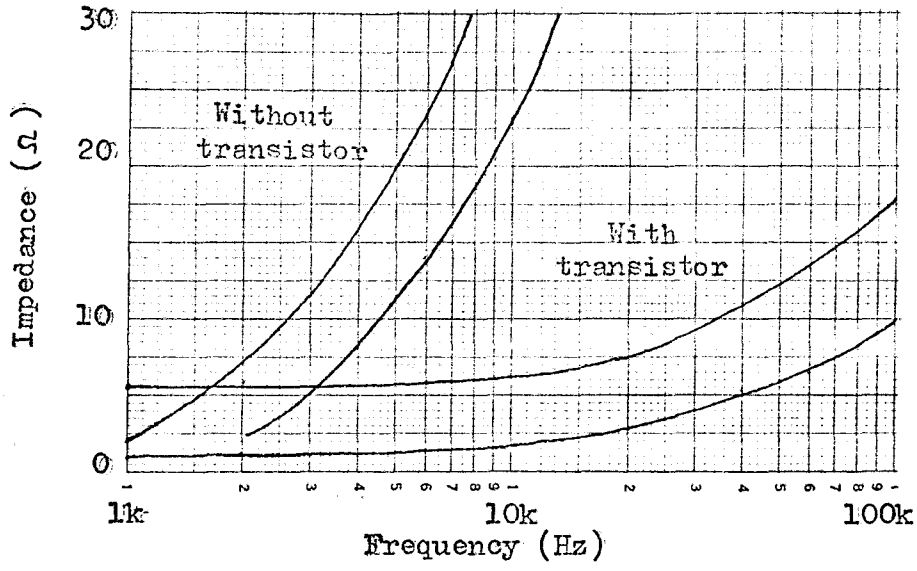

Fig. 18. Impedance between terminal E (or N) and the grid centre, with and without an additional transistor

(9) Overall linearity from the digital input to the analogue output at the floating circuit

A digital signal (zero to 63 in binary code) was fed into the input terminals of a DAC in the input memory, and the output voltage (with level compensation) of the emitter of the photo-transistor in an opto-electronic coupler used for a grid card was measured. Fig. 19 shows the result which is satisfactory.

(10) Combined operations of the Coriolis force and external force

A sine-wave electric current representing a water current (in fact a volume transport) in N-S (or E-W) component was fed between the corresponding terminals of a grid card, and at the same time another triangle or square wave voltage representing an external force was fed into the external-force terminals (N or W), then the voltage between one of the output terminals and the grid centre was measured. Fig. 20 shows the results which are satisfactory.

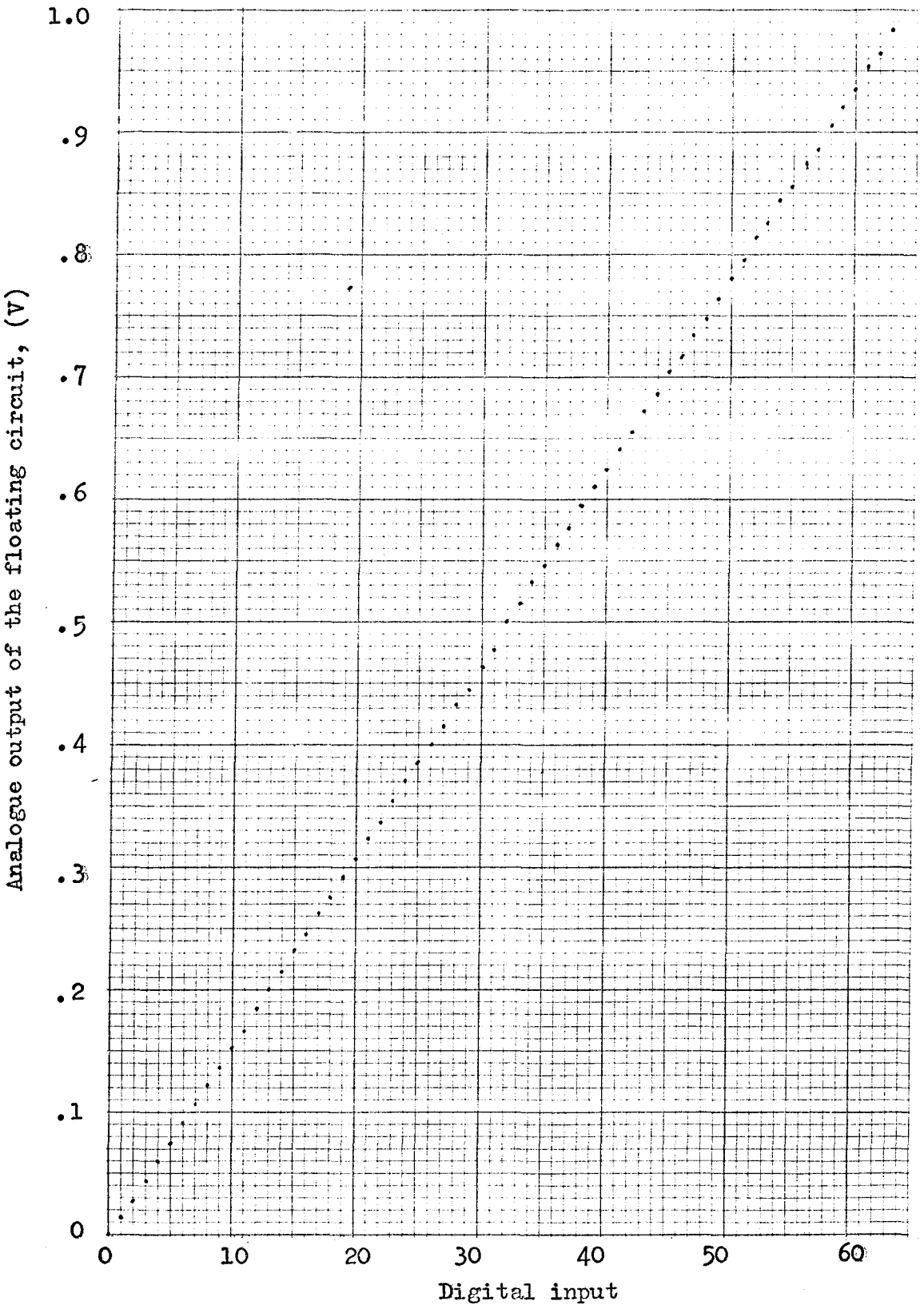

Fig. 19 Overall linearity from the digital input of the input memory to the analogue output of the floating circuit, through the opto-electronic coupler.
(The analogue output voltage was measured by a DVM having an accuracy of ± 0.1%).

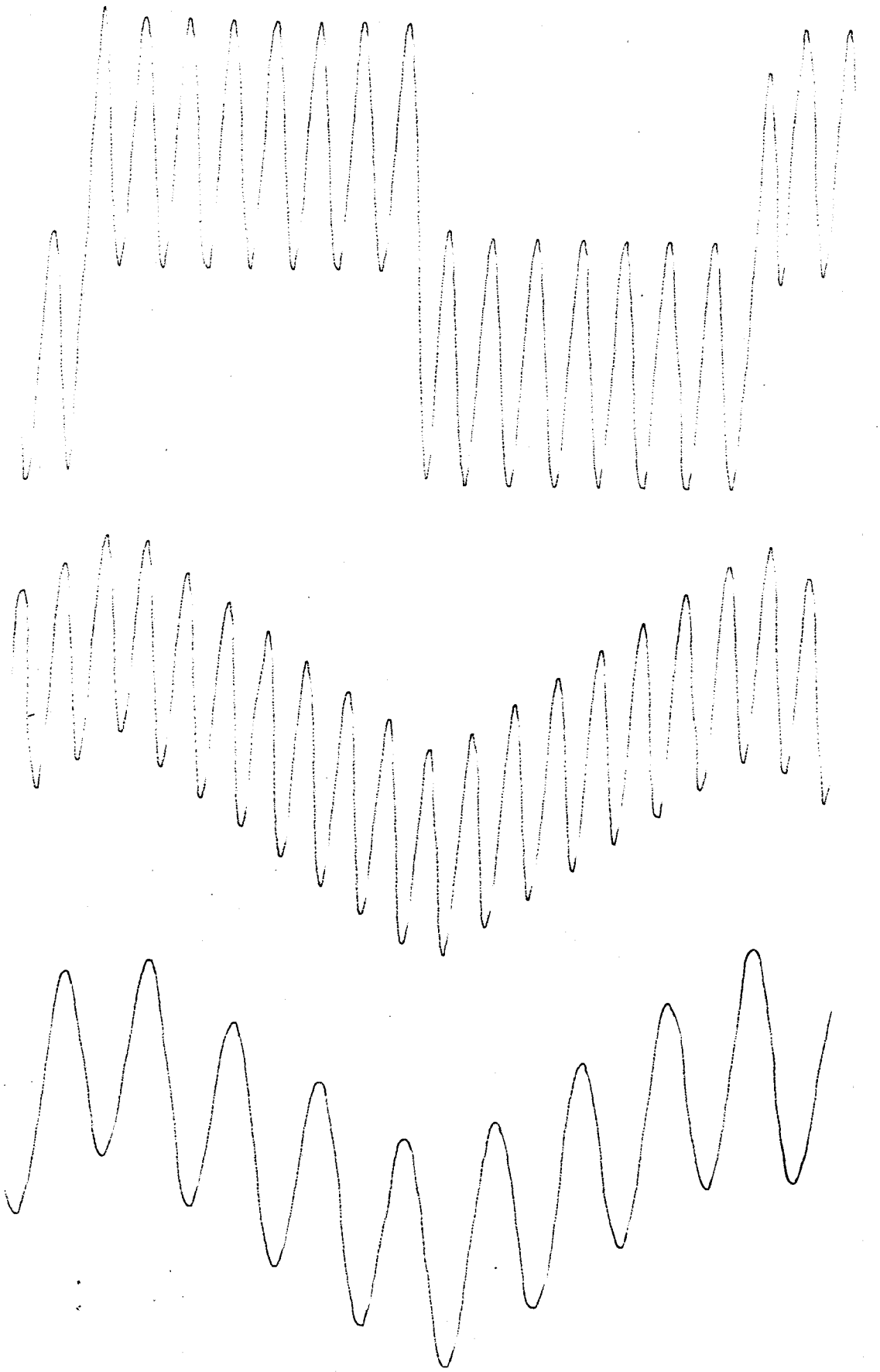

Fig. 20. Examples of combined waveforms of the Coriolis force and external force measured at the centre of a grid. In order to distinguish the two types of force, different waveforms and/or frequencies were used.

(11) Common-mode voltage rejection

All the OAs used for a grid card have differential inputs so that common-mode voltages are rejected. The degree of the rejection depends on the matched pair of resistors or capacitors concerned. By feeding a common-mode sine-wave voltage of 1V peak-to-peak at various frequencies into the input, voltages between terminal N (or E) and the grid centre were measured. Fig. 21 shows example of the results. At 4 kHz, the unbalanced voltage for the N component is not measurable, and that for the E component is about 0.02% of the common-mode voltage.

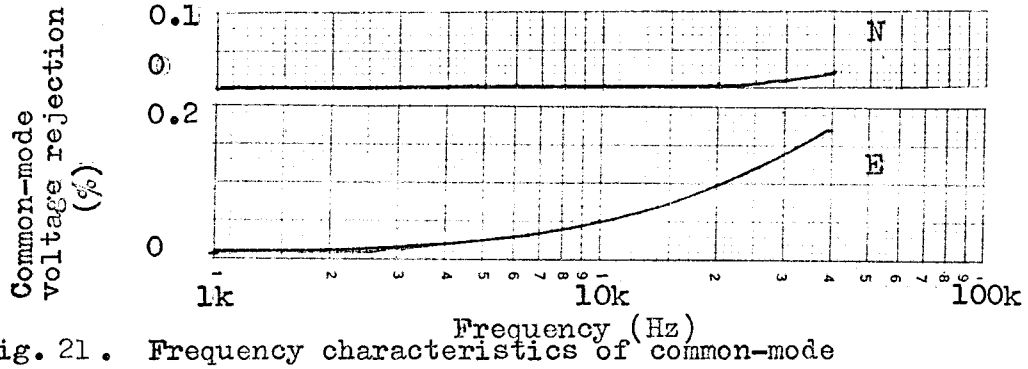

Fig. 21. Frequency characteristics of common-mode voltage rejection.

(12) Temperature stability

By choosing the S and N components which has no opto-electronic coupler, output-voltage level change due to ambient temperature was tested. Fig. 22 shows the results. The change is less than +4 mV, which is 1.3% of the full scale specified in Table 5, against the temperature change of 25°C ± 10°C. Refering to the ambient temperature change described in 4.1.2(1), this is satisfactory.

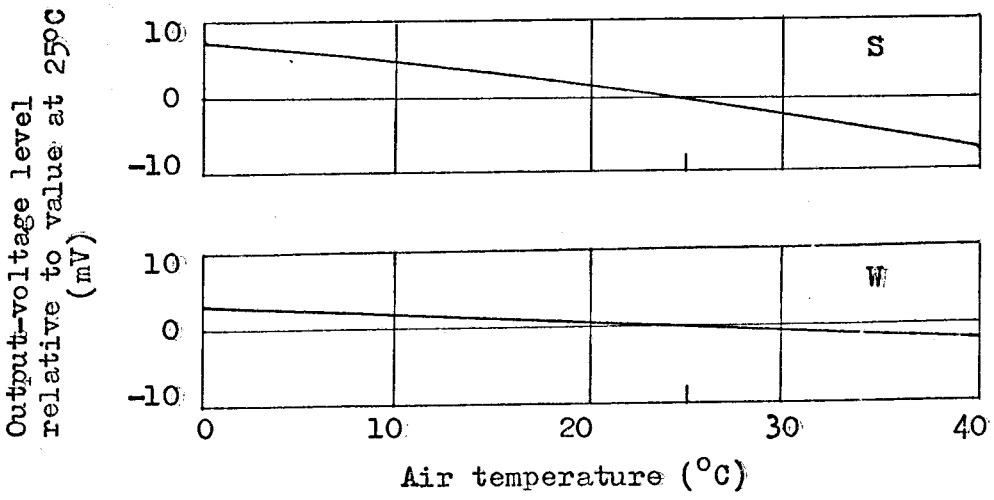

Fig. 22. Output-level change in the S and W units (opto-electronic couplers are not included) due to temperature change, relative to value at 25°C.

11. CONCLUSION

New 'grid cards' and their floating DC-power supply units have been designed and tested successfully. 330 sets of cards and power supply units have been manufactured.

ACKNOWLEDGEMENTS

The author wishes to thank Mr. John Smithers for his assistance in testing and manufacturing the grid cards and floating DC-power supply units. The author also wishes to thank Mr. John Bunting for his effort in manufacturing the floating DC-power supply units.

APPENDIX 1

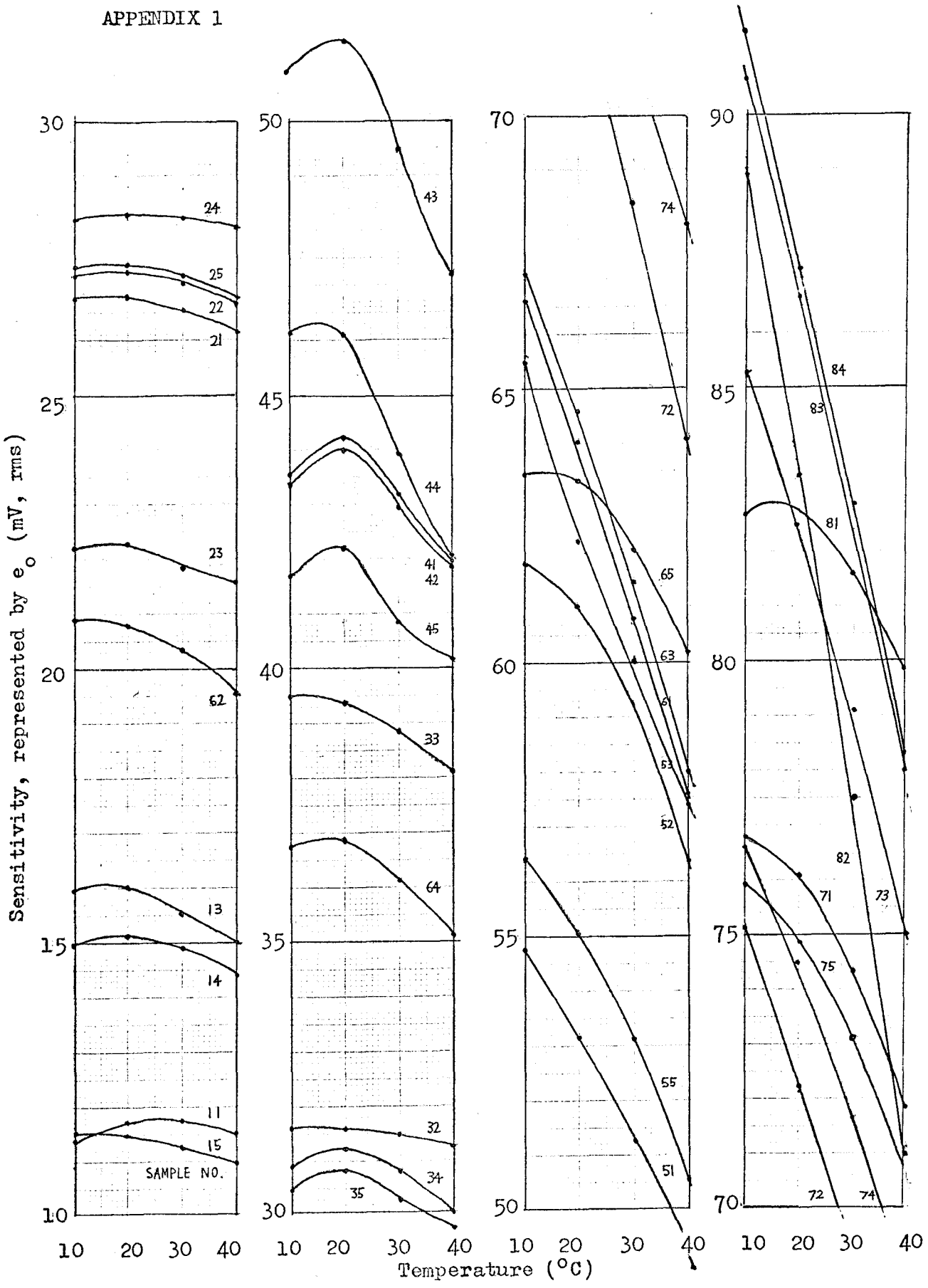

Examples of the ac-signal sensitivity change of opto-electronic couplers due to ambient temperature (10°C to 40°C), tested by the circuit shown in Appendix 2. About five samples per each sensitivity group are shown.

APPENDIX 2

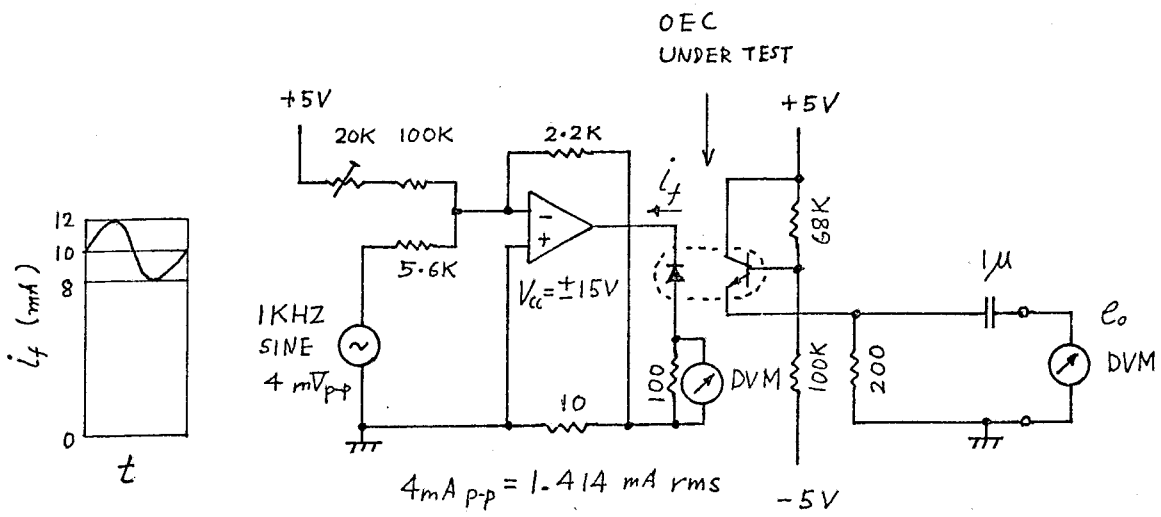

OECs under test only were set in a temperature-controlled chamber.

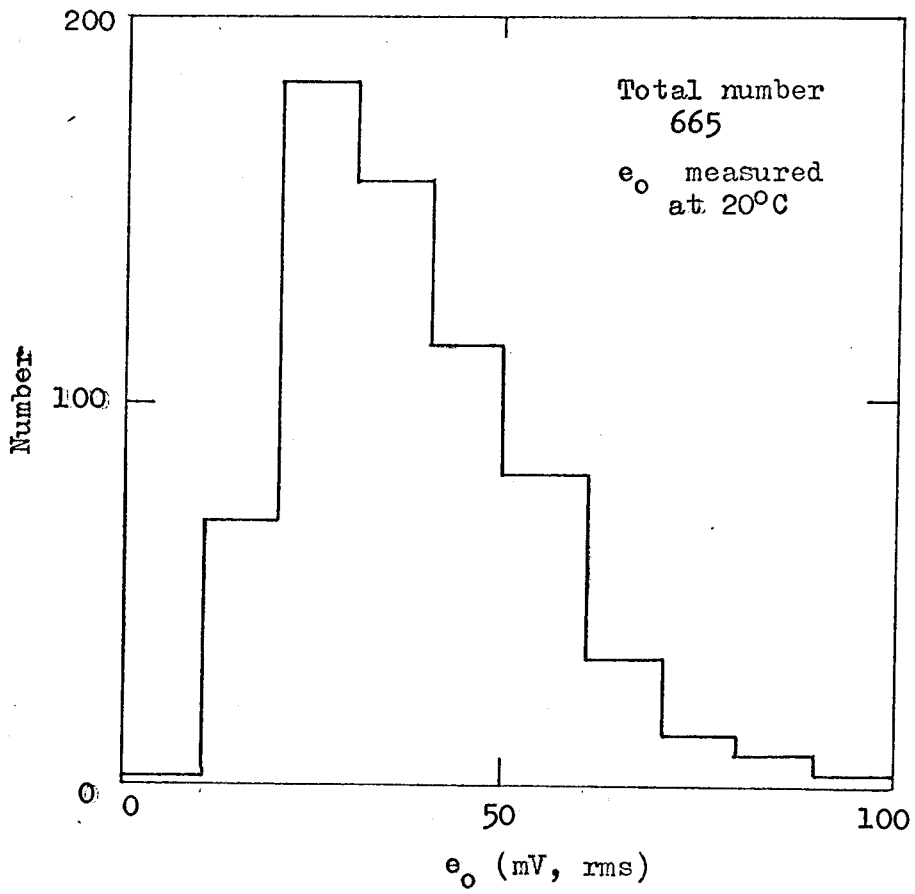

Number of opto-electronic couplers, Type TIL-112, against the relative sensitivity, and the test circuit.

APPENDIX 3 Manufacturing deviation of high-frequency characterisics of 747C measured for designing the grid cards.

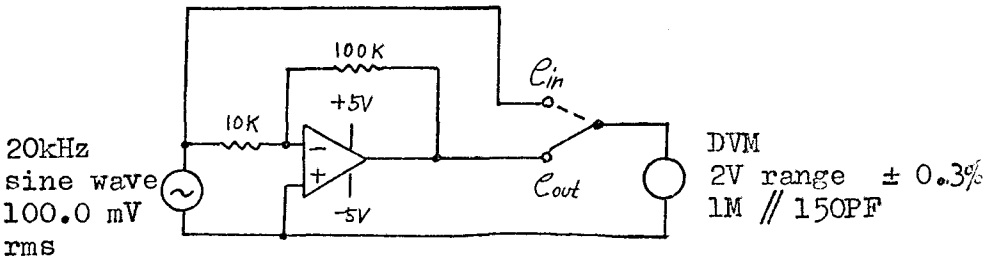

Measuring circuit

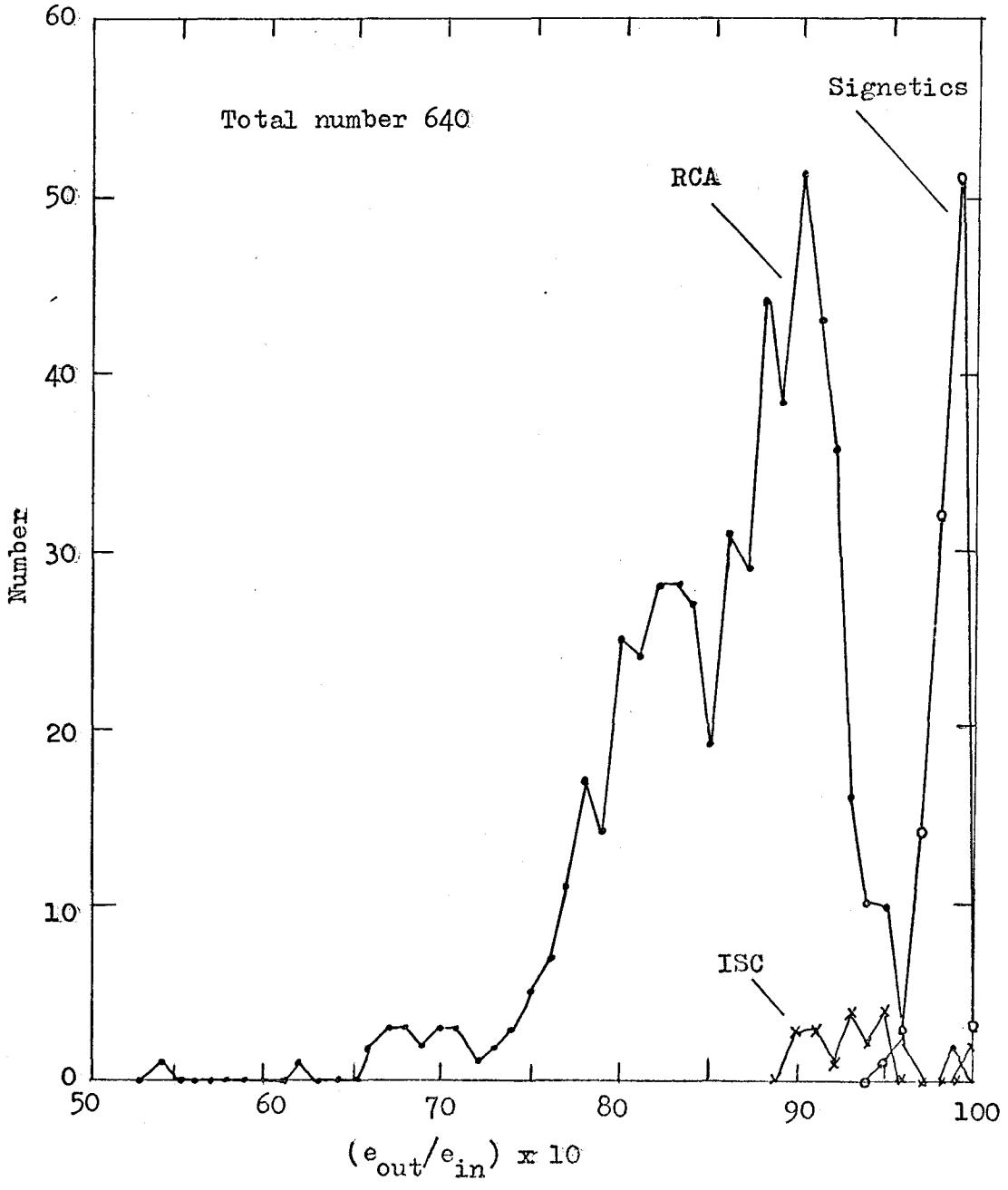

APPENDIX 4 Manufacturing deviation of solid-state tantalum capacitors.

Type ITT TAG-33/3, Nominal capacitance 33 μF, Working voltage 3V, Surege voltage 3.5V, Reverse polarisation 0.3V

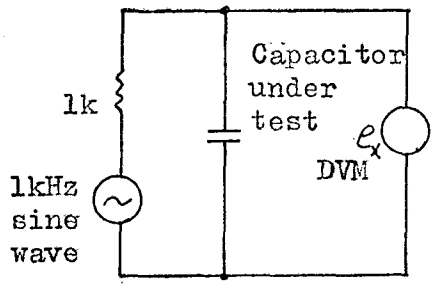

Standard capacitor 28.0 μF

Ambient temperature 23.5°C

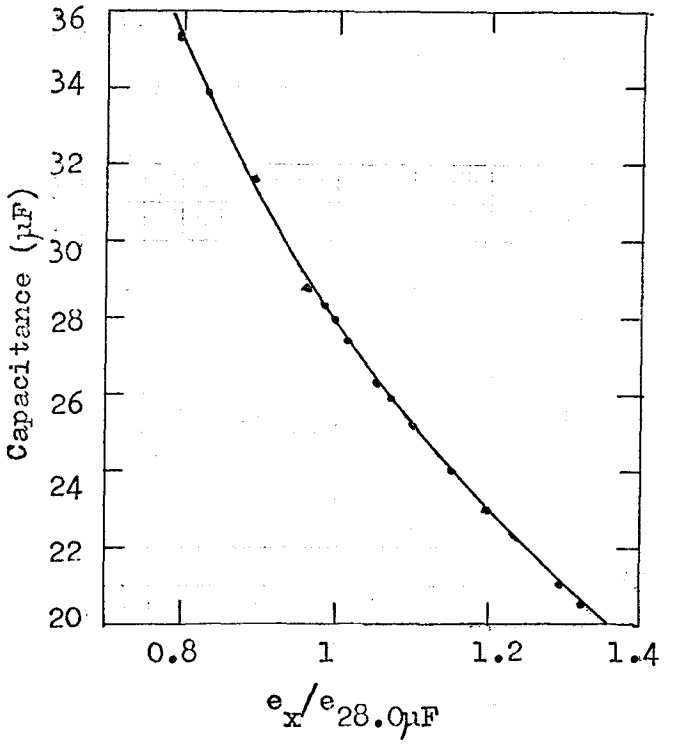

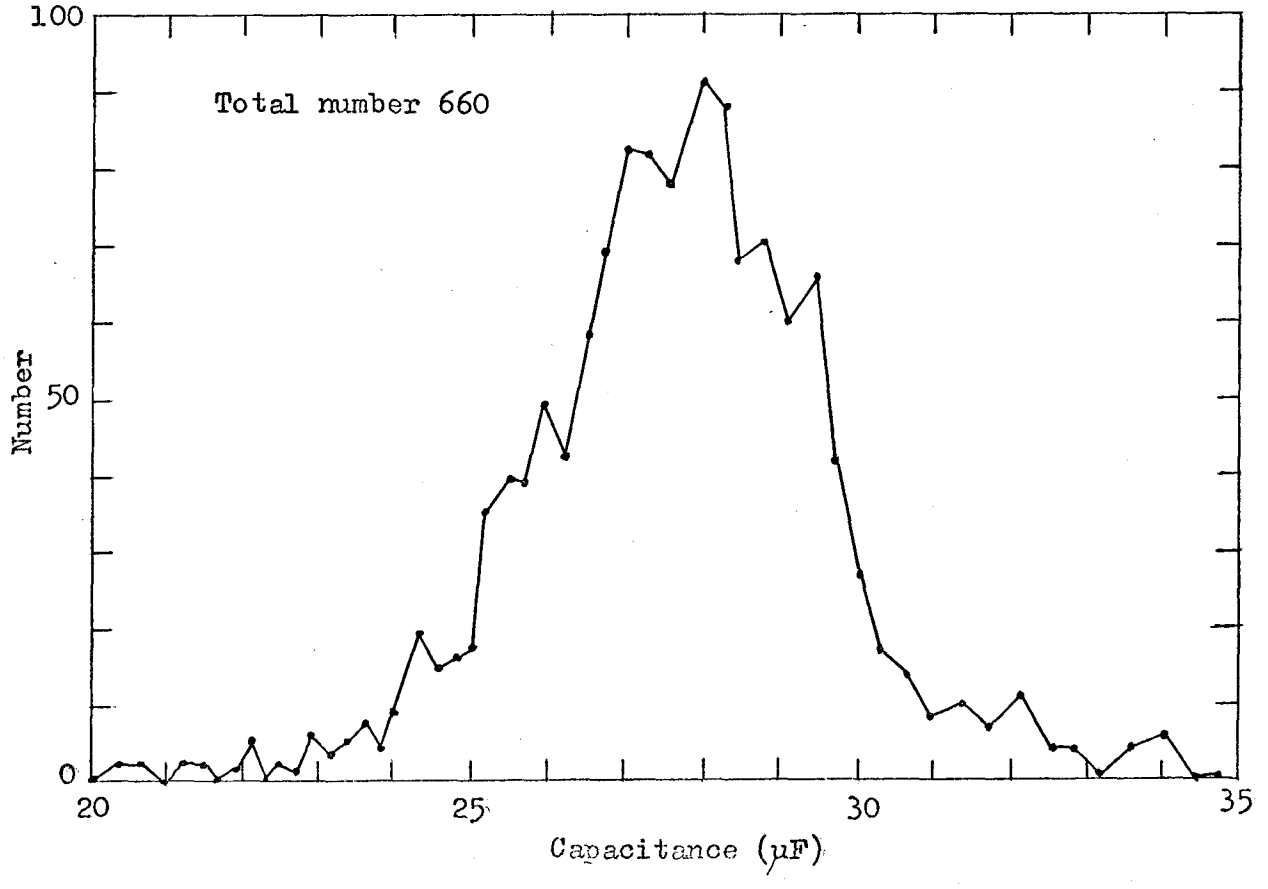

APPENDIX 5 Physical design of the floating-dc power supply

1. Winding The primary and secondary windings are identical, except for their leads. Each winding is made of 500 turns of 35 SWG 'Lewmexbond' enamelled copper wire. The wire wound on a former is heated by a current of 3A (dc or ac rms) for 15 sec so that the winding becomes self-supporting (each winding has resistance of 15Ω).

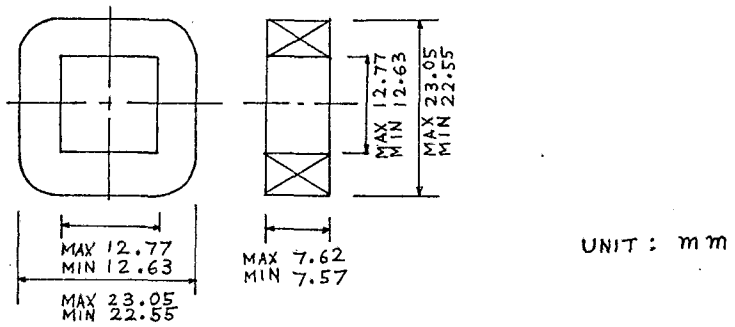

2. Screen foil for windings Electrically-insulated liquid vinyl 'Vycoat' is sprayed on the whole of one side and a part of the other side (shaded area in the drawing) of the aluminium foil, and cut to the specified dimensions.

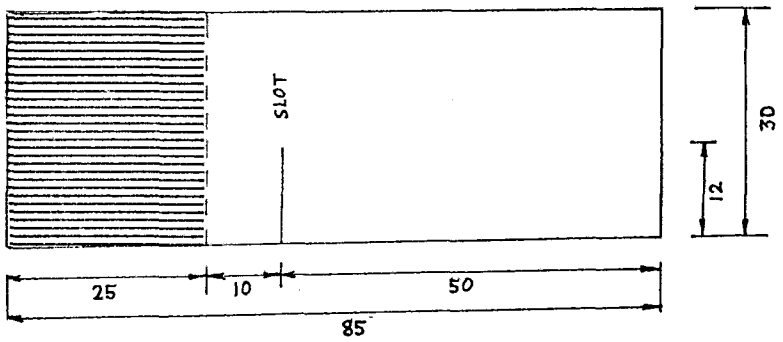

3. Leads Lead P is used for the primary winding, and Lead S for linking the secondary winding and the PC board. All conductors used for the leads are PVC covered 10/0.1 mm tinned copper; colours Red, Blue, and Green (earth). Each lead is screened by a very dense (ideally 100%) tinned-copper-net screen, and covered by varnished silk tape held with 'Evostik'. IMPORTANT: These screens affect the quality of the whole system seriously. Standard twin screened wire (RS Type Min Mike Twin) is used for Lead D. A green lead is soldered to each screen. Each of Leads P and D is terminated by a connector pin (Cambion Type 1521-3-03) with a silicon rubber sleeve.

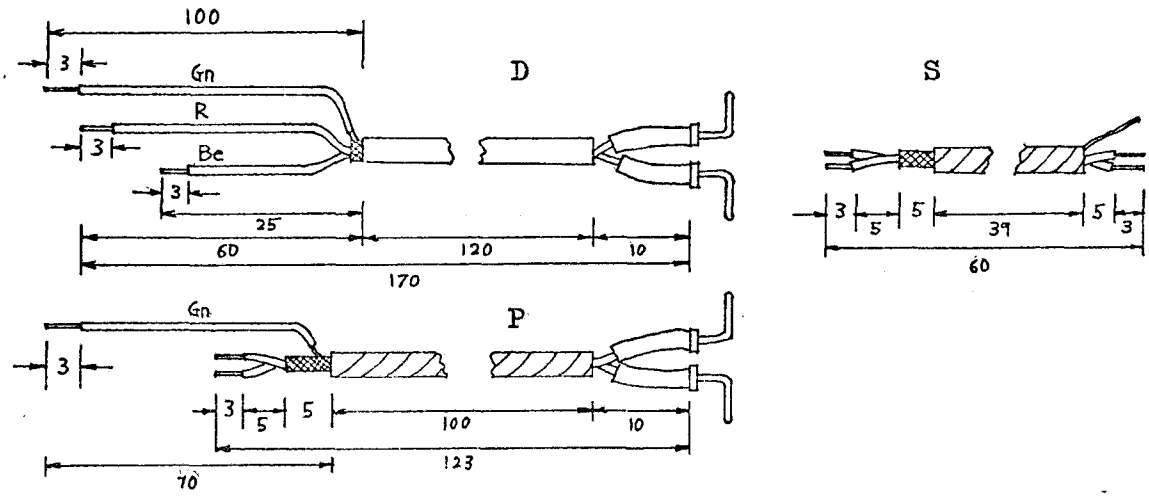

4. Insulation of joints of leads Soldered joints between the winding and leads are insulated by thermosetting tape by which the leads are secured physically at the same time.

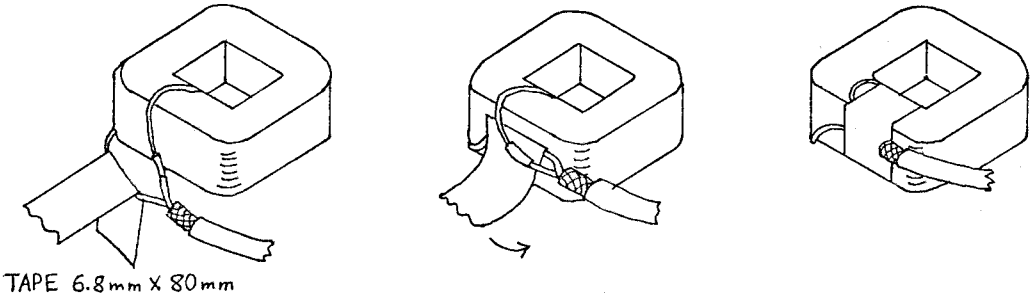

5. Screening of windings Each winding is screened by the foil described in 2, by using a jig. The foil, screen of the leads, and earth lead are soldered at a point using aluminium flux. The screened winding is bound by varnished silk tape, and held at its end with 'Evostik'. IMPORTANT: (1) No part of the winding or leads must be exposed outside the screen, since this affects the quality of the whole system. (2) The foil must not make an electrically closed circuit around the winding.

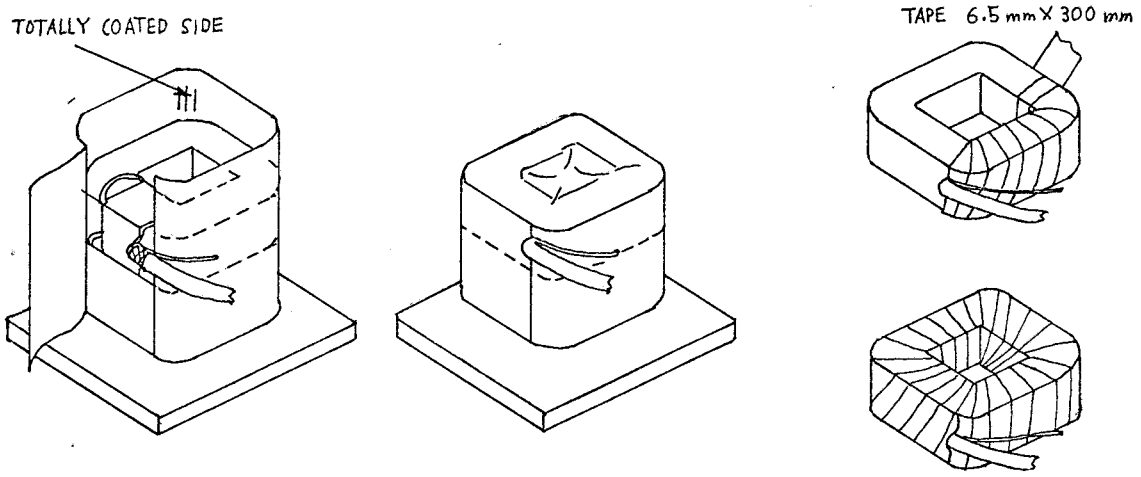

6. Transformer core Belclere Type GN-Unisil (33 laminations) whithout the standard frame (the maximum electo-magnetic power-transmission capacity 2 W) is used.

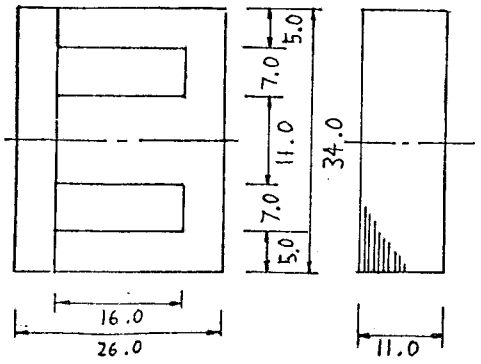

7. Components on the PC board All the components are mounted on one side of the board, except for two capacitors (both 250 μF, 25V) which are mounted on the other side.

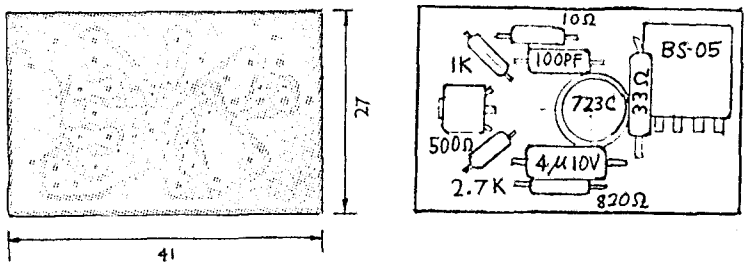

8. Inner screen Copper foil formed by a jig is joined by PVC tape (19 mm wide) which acts as an insulator against the transformer core.

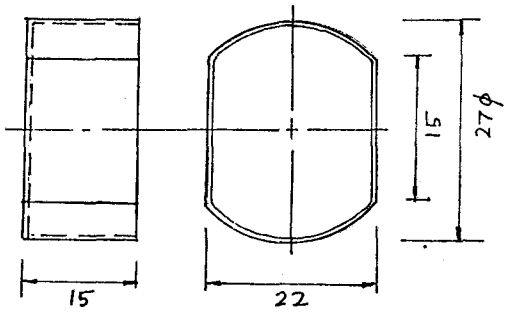

9. Case and related parts The case is made of a standard aluminium container (H.S. Sanders Ltd., 30 mmØ, 140 mmL) cut to 85 mmL, with a fixing hole (9.5 mmØ) drilled at the bottom. The cap is made of aluminium for the purpose (22 SWG, 30 mmØ inside, 10 mmL), A screw bush (9.5 mmØ, 12 mmL) and a lock washer with solder tag are used for fixing through the hole.

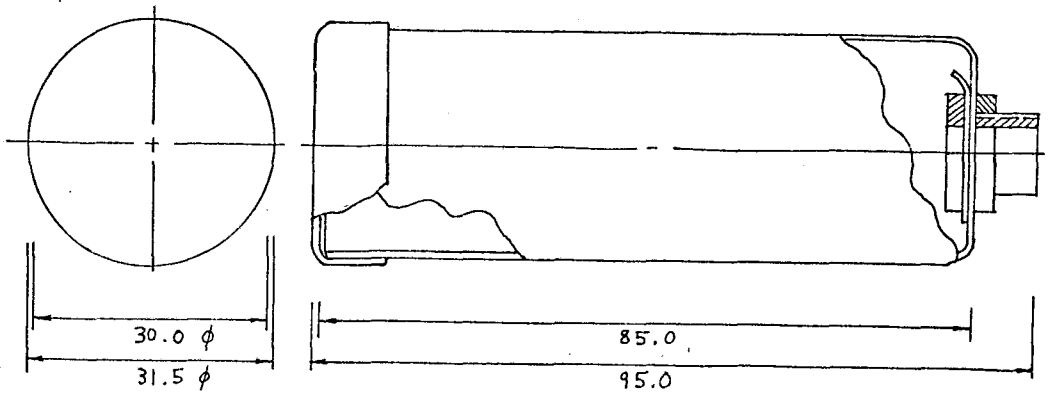

10. Assembly Assembled components are shown in the drawing. Positions of leads relative to the transformer should be kept strictly as specified, since this arrangement minimizes noise in the output. The order of the assembly is as follows:-

(1) Lead D is soldered to the PC board.
(2) The primary and secondary windings are assembled with the core. The laminations of the core must be exactly 33. They are bound tightly by electrical selotape (Scotch, 6 mm wide) at two edges of the core.
(3) A plastic sponge pad (20 mm x 20 mm x 5 mm) with adhesive is stuck on one side of the core.
(4) Lead S is soldered to the PC board.
(5) The inner screen is soldered to the PC board at a point (marked by * in the drawing).
(6) Leads P and D are inserted through the bush and washer.
(7) The green leads attached to Leads P and D are soldered to the PC board at a point (marked by + in the drawing).
(8) All the above components, except for the bush and washer, are covered tightly by varnished silk (85 mm x 100 mm), and its edges are joined by 'Evostik'.
(9) The above assembled parts are inserted into the case so that the bush and washer with Leads P and D pass through the fixing hole of the case. The bush is tightened with a nut applied from the outside of the case. The cap is fitted.

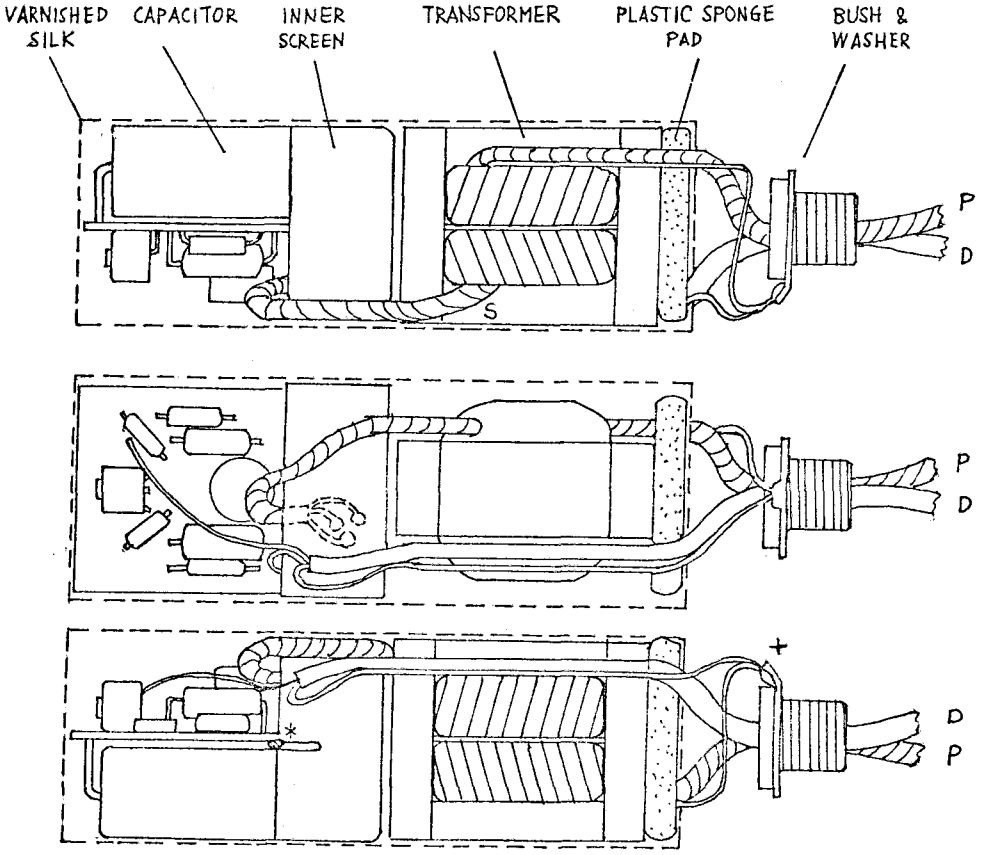

Full scale

APPENDIX 6 : Design of variable inductors.

Common for Types 1 to 4	ν = 0.010 a_μ = 0.040 Δa_μ = 0.050 ε_μ = 0.030 m = 3 C_1 = 5.58 cm^{-1} μ_{eN} = 90.62	Core : LL2501 Coil former: DT2178 Board : DT2359 Clips : DT2399 Adjuster : LA1295 (Mullard Vinkor)

	Types 1 & 2	Types 3 & 4	Type-1	Type-2	Type-3	Type-4
h_{min} h_{max}	Water-depth range (m) →		9.7 21.6	21.2 47.0	46.0 100	99.8 211
ε_N	0.005	0.010	Number of turns			
	Ratio to N_1					
N_1	1.0000	1.0000	1980 ± 4	1347 ± 3	915 ± 4	625 ± 3
N_2	0.86875	0.87256	1720 ± 4	1170 ± 2	798 ± 2	545 ± 2
N_3	0.75472	0.76135	1494 ± 3	1017 ± 2	697 ± 3	476 ± 2
Wire gauge *	SWG →		45	43	41	39
R_1	Culculated dc resistance → (ohms)		314	129	58.4	28.7
R_2			273	112	50.8	25.0
R_3			237	92.4	44.4	21.8
	Ratio to L_1		Inductance (H)			
L_{max}	1.3047	1.2998	1.0437	0.4827	0.2210	0.1039
L_{1max}	1.3450	1.3400	1.0760	0.4977	0.2278	0.1072
L_{1min}	1.0050	1.0100	0.8040	0.3719	0.1717	0.08086
L_1	1.0000	1.0000	0.8000	0.3700	0.1700	0.08000
L_{2max}	1.0152	1.0202	0.8120	0.3756	0.1734	0.08162
L_{2min}	0.7585	0.7689	0.6068	0.2806	0.1307	0.06152
L_2	0.7548	0.7613	0.6038	0.2793	0.1294	0.06091
L_{3max}	0.7662	0.7767	0.6130	0.2835	0.1320	0.06214
L_{3min}	0.5725	0.5854	0.4580	0.2118	0.09953	0.04684
L_3	0.5697	0.5796	0.4557	0.2108	0.09854	0.04637
Lmin	0.5897	0.6030	0.4717	0.2182	0.1025	0.04824

* Enamelled copper wire to BS1844 (fine covering)